ACS Catalysis

Research Article

Cite This: ACS Catal. 2018, 8, 2995−3010

pubs.acs.org/acscatalysis

Consequences of Confinement for Alkene Epoxidation with Hydrogen Peroxide on Highly Dispersed Group 4 and 5 Metal Oxide Catalysts

Daniel T. Bregante,[†] Nicholas E. Thornburg,[‡,§] Justin M. Notestein,[‡] and David W. Flaherty*[,†]

[†]Department of Chemical and Biomolecular Engineering, University of Illinois at Urbana−Champaign, Urbana, Illinois 61801, United States

[‡]Department of Chemical and Biological Engineering, Northwestern University, Evanston, Illinois 60208, United States

Supporting Information

ABSTRACT: Ti, Nb, and Ta atoms substituted into the framework of zeolite *BEA (M-BEA) or grafted onto mesoporous silica (M-SiO_2) irreversibly activate hydrogen peroxide (H_2O_2) to form pools of metal-hydroperoxide (M-OOH) and peroxide (M-(η^2-O_2)) species for alkene epoxidation. The product distributions from reactions with *Z*-stilbene, in combination with time-resolved UV−vis spectra of the reaction between H_2O_2-activated materials and cyclohexene, show that M-OOH surface intermediates epoxidize alkenes on Ti-based catalysts, while M-(η^2-O_2) moieties epoxidize substrates on the Nb- and Ta-containing materials. Kinetic measurements of styrene (C_8H_8) epoxidation reveal that these materials first adsorb and then irreversibly activate H_2O_2 to form pools of interconverting M-OOH and M-(η^2-O_2) intermediates, which then react with styrene or H_2O_2 to form either styrene oxide or H_2O_2 decomposition products, respectively. Activation enthalpies ($\Delta H^{\ddagger}$) for C_8H_8 epoxidation and H_2O_2 decomposition decrease linearly with increasing heats of adsorption for pyridine or deuterated acetonitrile coordinated to Lewis acid sites, which suggests that materials with greater electron affinities (i.e., stronger Lewis acids) are more active for C_8H_8 epoxidation. Values of $\Delta H^{\ddagger}$ for C_8H_8 epoxidation and H_2O_2 decomposition also decrease linearly with the ligand-to-metal charge-transfer (LMCT) band energies for the reactive intermediates, which is a more relevant measure of the requirements for the active sites in these catalytic cycles. Epoxidation rates depend more strongly on the LMCT band energy than H_2O_2 decomposition rates, which shows that more electrophilic M-OOH and M-(η^2-O_2) species (i.e., those formed at stronger Lewis acid sites) give both greater rates and greater selectivities for epoxidations. Thermochemical analysis of $\Delta H^{\ddagger}$ for C_8H_8 epoxidation and adsorption enthalpies for C_8H_8 within the pores of *BEA and SiO_2 reveal that the 0.7 nm pores within M-BEA preferentially stabilize transition states for C_8H_8 epoxidation with respect to the 5.4 nm pores of M-SiO_2, while H_2O_2 decomposition is unaffected by the differences between these pore diameters due to the small Stokes diameter of H_2O_2. Thus, the differences in reactivity and selectivity between M-BEA and M-SiO_2 materials is solely attributed to confinement of the transition state and not differences in the identity of the reactive intermediates, mechanism for alkene epoxidation, or intrinsic activation barriers. Consequently, the rates and selectivities for alkene epoxidation reflect at least two orthogonal catalyst design criteria—the electronegativities of the transition metal atoms that determine the electronic structure of the active complex and the mean diameters of the surrounding pores that can selectively stabilize transition states for specific reaction pathways.

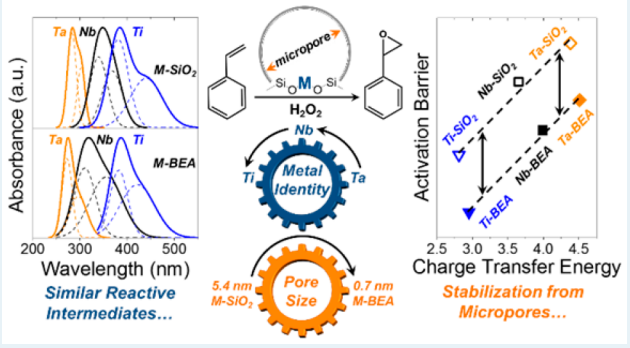

KEYWORDS: *titanium, niobium, tantalum, epoxidation, hydrogen peroxide, reactive intermediates, solvation*

1. INTRODUCTION

Highly dispersed metal oxides are ubiquitous in the selective oxidation of various alkanes, alkenes, aromatics, alcohols, and aldehydes to produce both commodity and fine chemicals.[1−3] The production of epoxides from alkenes is important, because epoxides are precursors for the manufacture of plastics, fragrances, and pharmaceuticals.[4−6] In recent years, a number of studies have investigated the use of highly dispersed group 4 and 5 metal oxides (e.g., grafted onto mesoporous silica[7,8] or incorporated into a zeolite framework[9,10]) to activate hydrogen peroxide (H_2O_2) for epoxidation reactions.[11] The interest in H_2O_2 is motivated, in part, by the lower environmental impact for the use of this oxidant in comparison to Cl_2 (e.g., used in the chlorohydrin process)[12] and organic oxidizers (e.g., *tert*-butyl hydroperoxide and ethylbenzene hydroperoxide).[13] Epoxidations that utilize H_2O_2 form only H_2O as a byproduct

Received: November 22, 2017
Revised: January 18, 2018
Published: February 15, 2018

DOI: 10.1021/acscatal.7b03986
ACS Catal. 2018, 8, 2995−3010

and, hence, do not require the regeneration or sale of organic co-products nor the remediation of environmentally impactful waste streams.

Large amounts of titanium silicalite (TS-1) are used in the hydrogen peroxide-propylene oxide process to catalyze the activation of H_2O_2 and the epoxidation of propylene.[14,15] However, many other monomeric metal centers and small oligomers of metal oxides (e.g., Al,[16,17] Ti,[7,18−20] Zr,[7,21] Nb,[9,22,23] and Ta[24−26]) activate H_2O_2 and catalyze alkene epoxidations as well. Recent reports from our group show that the rates and selectivities for cyclohexene epoxidation increase with increasing heat of adsorption for Lewis acid bound deuterated acetonitrile, which suggests that materials that possess greater electron affinities (i.e., stronger Lewis acids) are more productive catalysts for this chemistry.[9,10,27] Despite the plethora of literature on the epoxidation of alkenes with H_2O_2,[22,28−30] the changes in rates and selectivities that result from differences in the electronic structure due to changing pore environment (e.g., type or morphology of support) and changes in the solvating environment (i.e., catalyst pore diameter) have not been fully described in the open literature, to the best of our knowledge.

Here, we seek to establish and explain the relationships that exist between the rates and selectivities for alkene epoxidation and the electronic structure of the reactive intermediates and morphological properties (e.g., metal atom coordination and mean pore diameters) of two series of catalysts that contain monomeric Ti, Nb, or Ta atoms on siliceous supports. The two categories of materials consist of transition metal atoms (Ti, Nb, or Ta) incorporated into the framework of zeolite *BEA (M-BEA)[10] or those same atoms grafted onto mesoporous silica (M-SiO_2).[7] UV−vis spectra obtained in situ suggest that all materials irreversibly activate H_2O_2 to form pools of M-OOH and M-(η^2-O_2) intermediates. Transient in situ UV−vis spectra obtained during reaction of these species with cyclohexene, in conjunction with the isomeric distribution of the products from *Z*-stilbene epoxidation, show that Ti-BEA and Ti-SiO_2 catalysts react through M-OOH, while Nb and Ta materials epoxidize cyclohexene through M-(η^2-O_2). Changes in the rates of styrene (C_8H_8) epoxidation and H_2O_2 decomposition as functions of reactant concentrations show that the active M-OOH and M-(η^2-O_2) intermediates form following adsorption and irreversible activation of H_2O_2, after which these species react with C_8H_8 or H_2O_2 to form the epoxidation or decomposition products, respectively. Epoxidation and H_2O_2 decomposition rates and selectivities depend exponentially on the extent of electron exchange between the reactive intermediate and the metal atom, as assessed by the ligand-to-metal charge-transfer (LMCT) energy measured via UV−vis. Activation enthalpies ($\Delta H^{\ddagger}$) for C_8H_8 epoxidation are systematically lower on M-BEA materials than M-SiO_2 by ∼20 kJ mol^{-1}, while $\Delta H^{\ddagger}$ for H_2O_2 decomposition do not depend on the type of silica support used. Thermochemical analysis of the values of $\Delta H^{\ddagger}$ for C_8H_8 epoxidation and the adsorption enthalpies for C_8H_8 adsorption into the purely siliceous materials show that transition states for C_8H_8 epoxidation are preferentially stabilized within the microporous *BEA framework relative to those in mesoporous SiO_2, while transition states for H_2O_2 decomposition are not affected because the Stokes diameter of H_2O_2 (∼0.24 nm) is too small to be significantly stabilized by dispersive interactions with the pore walls of these materials. Consequently, the design of materials that maximize the extent of solvation of the desired alkene reactant in the microporous voids will result in a catalyst with increased rates and selectivities for this chemistry.

2. MATERIALS AND METHODS

2.1. Catalyst Synthesis. All M-BEA and M-SiO_2 catalysts used in this study have been synthesized and characterized by the authors within previous reports.[7−10] The most relevant results are summarized here, with additional characterization data and interpretation provided in the Supporting Information (SI), section S1.

M-BEA catalysts were prepared by the liquid-phase postsynthetic modification of commercially available NH_4^+-BEA (Zeolyst, CP814E).[9,10,18,31−33] In short, NH_4^+-BEA (Si:Al ∼ 12.5) was dealuminated by reflux in concentrated HNO_3 (Macron Chemicals, 68−70 wt%, 20 cm^3 g^{-1}) for 18 h. The solids were recovered by vacuum filtration and washed thoroughly with H_2O (17.8 MΩ·cm, 50 cm^3 g^{-1}) and heated at 5 K min^{-1} to 823 K in flowing air (Airgas, Ultra-zero grade, 100 cm^3 min^{-1}) and held for 6 h to produce Si-BEA (Si:Al >1200, determined by ICP-OES). The incorporation of Ti, Nb, or Ta atoms into the dealuminated framework involved stirring a suspension of Si-BEA in a solution of $TiCl_4$ (Sigma-Aldrich, 99.9%; *Caution! $TiCl_4$ will violently react with the moisture in air to form TiO_2 and HCl, and should be handled carefully*), $NbCl_5$ (Sigma-Aldrich, 99.9%), or $TaCl_5$ (Sigma-Aldrich, 99%) in dichloromethane (Fisher Chemicals, Certified ACS stabilized) for $TiCl_4$ or isopropanol (Fisher Chemicals, Certified ACS plus) for $NbCl_5$ and $TaCl_5$ at 333 K for 3 h. Volatile components were then removed by rotary evaporation. Recovered solids were heated at 5 K min^{-1} to 823 K in flowing air (Airgas, Ultra-zero grade, 100 cm^3 min^{-1}) and held for 6 h to produce the corresponding M-BEA catalyst. The metal loading within the catalysts was varied by changing the concentration of the MCl_x solution used during the liquid-phase treatments.

All M-SiO_2 materials were synthesized using standard glovebox and Schlenk techniques.[34−37] $TiCl_4(THF)_2$ (Strem Chemicals, >97% metals basis), $NbCl_5$ (Strem Chemicals, >99%), and $TaCl_5$ (Strem Chemicals, >99%) metal precursors were stored and weighed in an Ar glovebox. 1,3-Dimethoxy-*tert*-butylcalix[4]arene ("dmCalix") was prepared from *p-tert*-butylcalix[4]arene ("Calix", Sigma-Aldrich, >95%) according to previously published procedures.[38] Briefly, Ti-, Nb-, and Ta-calixarene complexes were synthesized by refluxing the metal chloride precursors with stoichiometric amounts of dmCalix (Ti) or Calix (Nb, Ta) in dry, degassed toluene under an N_2 atmosphere for 14 h. Then, partially dehydroxylated SiO_2 (Selecto Scientific, 32−62 μm particle size, 570 m^2 g^{-1}, 5.4 nm average pore diameter, treated at 573 K under dynamic vacuum (<5 Pa) for 10 h) was added to the flask, and the suspension was refluxed for an additional 24 h. Solids were vacuum-filtered and washed with fresh toluene, then Soxhlet-extracted with toluene, and dried under dynamic vacuum (<40 mTorr) to yield bright-orange (Calix-Ti-SiO_2 and Calix-Nb-SiO_2) or light-brown (Calix-Ta-SiO_2) solids. Calix-M-SiO_2 solids were then heated at 5 K min^{-1} to 823 K in flowing air (Airgas, Ultra-zero grade, 100 cm^3 min^{-1}) and held for 6 h to remove the calixarene ligands and produce highly dispersed M-SiO_2 materials (bleached white in appearance).

2.2. Catalyst Characterization. The metal contents (Table 1) of the M-BEA and M-SiO_2 materials was quantified using inductively coupled plasma-optical emission spectroscopy (ICP-OES), which was calibrated against known dilution

DOI: 10.1021/acscatal.7b03986
ACS Catal. 2018, 8, 2995−3010

Table 1. Band Edge Energies,[a] Metal Loadings,[b] Fraction of Active Metal,[c] and Enthalpies of Adsorption[d] for Pyridine (ΔH_{Py}) and CD_3CN (ΔH_{CD_3CN}) Coordinated to Lewis Acid Sites on M-BEA and M-SiO_2 Catalysts

sample	band edge (eV)	metal loading (mmol g^{-1})	active metal (%)	ΔH_{Py} (kJ mol^{-1})	ΔH_{CD_3CN} (kJ mol^{-1})
Ti-BEA	4.0	0.22	96 ± 5	−45 ± 3	−31 ± 2[g]
Nb-BEA	4.2	0.16	99 ± 8	−25 ± 3	−22 ± 2[g]
Ta-BEA	4.8	0.16	99 ± 4	−20 ± 3	−17 ± 1[g]
Ti-SiO_2	3.8	0.18	77 ± 10[f]	−34 ± 4	−[e]
Nb-SiO_2	4.0	0.18	60 ± 7[f]	−16 ± 2	−[e]
Ta-SiO_2	4.5	0.19	60 ± 5[f]	−11 ± 2	−[e]

[a]Measured using DRUV−vis. [b]Measured by ICP-OES. [c]Determined by in situ methylphosphonic acid (for M-BEA) and phenylphosphonic acid (for M-SiO_2) titrations. [d]Determined from adsorption isobars using FTIR. [e]Not measured because CD_3CN readily cokes on M-SiO_2 at temperatures >373 K. [f]Reference 8. [g]Reference 10.

standards. M-BEA materials were synthesized to produce ∼0.6−1 M atom (unit cell)$^{-1}$. Consequently, statistical arguments suggest that the majority of transition metal atoms are well separated and that each unit cell of the M-BEA materials contains ∼4−5 silanol nests on average (after postsynthetic modification), which results in highly hydrophilic pores and external surfaces.

The crystallinity of each M-BEA material was confirmed by powder X-ray diffraction using a diffractometer (Siemens/Bruker, D5000) with Cu Kα radiation (0.15418 nm) under ambient conditions. Figure S1 shows the X-ray diffractograms of all M-BEA. The similarities between the diffractograms for all M-BEA suggests that the *BEA framework is intact after postsynthetic modification.

Band edge energies (E_g) for each M-BEA and M-SiO_2 material were determined from extrapolation of the linear portion of the corresponding Tauc plot calculated from diffuse reflectance UV−vis spectra (DRUV−vis) (Figure S2). Total reflectance spectra were measured at ambient conditions with a UV−vis−NIR spectrophotometer (Agilent CARY 5 for M-BEA; Shimadzu UV-3600 for M-SiO_2) with magnesium oxide (MgO, Sigma-Aldrich, 99.995%, for M-BEA) or polytetrafluoroethylene powder (for M-SiO_2) as a solid diluent and background. The relatively large band gaps (Table 1), and lack of significant shoulders on the absorbance features suggests that the transition metal atoms in *BEA and on SiO_2 are highly disperse and contain little oligomeric or bulk oxide phases. The Ta-SiO_2 material is the sole exception and possesses a small shoulder on the UV−vis absorbance spectra (Figure S2), which suggests that small TaO_x oligomers form upon oxidative heat treatments.[7] In this work, all reported rates were normalized by the fraction of *active* metal in the M-BEA and M-SiO_2 catalysts using in situ methylphosphonic acid (for M-BEA) or phenylphosphonic acid (for M-SiO_2) site titrations (see below).[8,39] Thus, the presence of TaO_x oligomers does not significantly affect reported rates.

The presence of Lewis acid sites in M-BEA and M-SiO_2 was characterized by the infrared (IR) spectra of adsorbed pyridine (Sigma-Aldrich, >99%) using a custom-built transmission cell[40] coupled to a Fourier transform infrared (FTIR) spectrometer (Bruker, Tensor 37) with a liquid-N_2-cooled HgCdTe detector. Catalysts were pressed into self-supporting disks (∼60 mg) and placed within the transmission cell, which was assembled using CaF_2 windows and connected to a gas manifold with lines heated to 423 K. All materials were first heated to 423 at 10 K min^{-1} and held for 2 h under flowing He (50 cm^3 min^{-1}; Airgas, Ultra-zero grade), with the intent to desorb water and residual organics. Pyridine (0.1 kPa; Sigma-Aldrich, 99%) was introduced via a syringe pump (KD Scientific, Legato 100) and vaporized in the heated gas-transfer lines into a stream of flowing He (50 cm^3 min^{-1}). Steady-state IR spectra (128 scans, 1 cm^{-1} resolution; Figure 1) of pyridine adsorbed to the M-BEA and M-SiO_2 samples were obtained while flowing the pyridine/He stream over the samples.

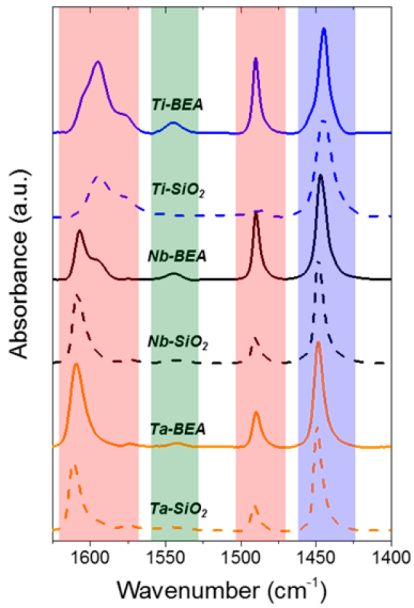

Figure 1. Infrared spectra of pyridine bound to Lewis and Brønsted acid sites on M-BEA (solid) and M-SiO_2 (dashed) materials containing Ti (blue), Ta (orange), or Nb atoms (black). All spectra are normalized to the feature at ∼1450 cm^{-1} and were acquired in flowing He (0.1 kPa pyridine, 50 cm^3 min^{-1}, ∼393 K). Colored regions along the horizontal axis denote the expected location of absorbance features for pyridine coordinated to only Brønsted acid sites (green), only Lewis acid sites (blue), and both Lewis and Brønsted acid sites (red).

Figure 1 shows steady-state IR spectra of pyridine adsorbed to M-BEA and M-SiO_2 materials (0.1 kPa pyridine, 50 cm^3 min^{-1} He, ∼393 K). All materials possess absorbance features between 1575 and 1625 cm^{-1} and at ∼1490 cm^{-1}, which are associated with pyridine coordinated to either Lewis or Brønsted acid sites (Figure 1, red region).[41−43] Yet, absorbance features at ∼1540 cm^{-1} arise only from pyridinium ions bound to Brønsted acid sites (Figure 1, green region).[41−43] These pyridinium ions likely bind to metal-hydroxyl species as observed for similar Ta-BEA materials,[43] however, M-BEA materials possess trace aluminum (Si:Al >1200 as detected by ICP-OES) and the Brønsted acid sites may be attributed to trace aluminum that remains in the framework. Absorbance features at ∼1450 cm^{-1} correspond only to pyridine bound to Lewis acid sites (Figure 1, blue region).[41−43] The enthalpies of pyridine adsorption (ΔH_{Py}) to Lewis acid sites were determined by van't Hoff analysis of the IR feature at ∼1450 cm^{-1} (Figure S3) to obtain one potential measure of the electron affinity (i.e., a measure of "Lewis acid strength") for each catalyst. Table 1 contains the experimentally determined values for ΔH_{Py} on all M-BEA and M-SiO_2 materials. Table 1

DOI: 10.1021/acscatal.7b03986
ACS Catal. 2018, 8, 2995−3010

also contains values for the enthalpy of adsorption for deuterated acetonitrile (ΔH_{CD_3CN}) coordinated to Lewis acid sites obtained using similar methodology by our group.[10]

X-ray photoelectron spectroscopy (XPS) was used to determine the oxidation state of transition metal atoms on bare and H_2O_2-activated Ti-, Nb-, and Ta-BEA and -SiO_2 materials. The XPS measurements were performed on a spectrometer (Kratos, AXIS Ultra) equipped with a monochromatic Al Kα (1486.6 eV) X-ray source. M-BEA and M-SiO_2 materials were activated with H_2O_2 by creating a slurry of catalyst (~60 mg) with a mixture of 2.5 cm^3 H_2O_2 (4.9 M; 30 wt% in H_2O; Fisher Scientific) in acetonitrile (CH_3CN; Macron Chemicals, >99.8%) and stirring at 333 K for 1 h. Volatile components were then removed in vacuo via a rotary evaporator (IKA, RV 10) and dried under dynamic vacuum for 12 h (~0.02 kPa). This treatment produced pale yellow solids from Ti and Nb materials and a cream colored solid for Ta catalysts. High-resolution X-ray photoelectron spectra were collected with a 40 eV pass energy, and the photoelectron binding energies were calibrated using the C 1s peak for aliphatic species at 284.8 eV. The Shirley background was subtracted, and peaks were fit using Gaussian curves.

Styrene (C_8H_8) adsorption enthalpies were measured by van't Hoff analysis of the change in C_8H_8 uptake into Si-BEA and SiO_2 as a function of temperature within the linear regime of the adsorption isotherm. A solution of C_8H_8 (Sigma-Aldrich, 99%) in CH_3CN was heated to a desired temperature while stirring in a 100 cm^{-3} round-bottom flask. An initial (solids-free) aliquot was taken and analyzed via gas chromatography (GC; HP 5890, Series A) to determine the initial concentration of C_8H_8. An appropriate amount of Si-BEA or SiO_2 was then added to the stirring solution of C_8H_8 and allowed to equilibrate at a given temperature. An aliquot of solution was then passed through a syringe filter (polypropylene, 0.22 μm) to remove the solids and was analyzed via GC. The difference in GC peak area between the aliquot after Si-BEA or SiO_2 introduction and the initial sample was assumed to be proportional to the amount of styrene adsorbed to the purely siliceous solids. Multiple concentrations of C_8H_8 were tested to determine a concentration that is well within the linear regime for the C_8H_8 adsorption isotherm (from 5×10^{-6} to 10^{-3} M [C_8H_8]). The uptake of C_8H_8 was then measured as a function of temperature to determine the enthalpies for adsorption of styrene from the CH_3CN solution to the siliceous support (ΔH_{ads}; Figure S4), and these values were found to be -35 ± 6 and -18 ± 3 for Si-BEA and SiO_2, respectively.

2.3. Measurement of Rates for Epoxide Formation and H_2O_2 Decomposition. Rates for C_8H_8 epoxidation and H_2O_2 decomposition were measured using batch reactors (100 cm^3, three-neck round-bottom flasks) equipped with reflux condensers to minimize evaporative losses. C_8H_8 and H_2O_2 (Fischer Chemicals, 30 wt% in H_2O) were added to a solution of CH_3CN and benzene (internal standard for GC analysis; Sigma-Aldrich, thiophene-free, >99%) and heated to the desired temperature (303–348 K) while stirring at 600 rpm. H_2O_2 (30% w/v) was distilled via rotary evaporation to produce ~90% w/v H_2O_2 and was combined with an appropriate amount of H_2O to quantify the effects of H_2O on styrene epoxidation rates. The reactions were initiated by addition of the M-BEA or M-SiO_2 catalysts and small aliquots (~300 μL) of the reaction solution were extracted as a function of time through a 0.22 μm syringe filter (to remove suspended catalyst and stop the reactions from proceeding). The concentrations of the organic components within these aliquots were quantified via a GC equipped with a flame-ionization detector. All species were identified and calibration factors were quantified using standards of known concentration. The concentration of H_2O_2 in each aliquot was measured by colorimetric titration using an aqueous solution of $CuSO_4$ (8.3 mM, Fisher Chemicals, >98.6%), neocuproine (12 mM, Sigma-Aldrich, >98%), and ethanol (25% v/v, Decon Laboratories Inc., 100%). The concentration of H_2O_2 was calculated by comparison of the absorbance at 454 nm to calibrated standards, measured using a visible-light spectrophotometer (Spectronic, 20 Genesys). Test reactions using purely siliceous Si-BEA and SiO_2 materials (0.01 M C_8H_8, 1 mM H_2O_2, 313 K) reveal that no reaction (i.e., epoxidation or H_2O_2 decomposition) occurs in the absence of the metal atoms.

The number of catalytically *active* metal atoms in M-BEA samples were determined using in situ site titrations with methylphosphonic acid (MPA; Sigma-Aldrich, 99%) during the epoxidation of cyclohexene (C_6H_{10}; Sigma-Aldrich, 99%).[8,39] Briefly, M-BEA was combined with a solution of MPA and C_6H_{10} with the intent for MPA to irreversibly bind to the active sites and inhibit epoxidation catalysis. An appropriate amount of H_2O_2 was then spiked into the reactor to initiate the reaction. Reactions were run with varying ratios of MPA-to-metal (MPA:M) where the MPA:M ratios that correspond to extrapolated turnover rates of zero are taken to be the fraction of active metal in M-BEA (Table 1; see SI, section S1.2). Cyclohexene epoxidation on all M-BEA produced only cyclohexene oxide, as no other oxidation products (e.g., cyclohexenone, 1-cyclohexen-3-ol, cyclohexanediol) were observed under differential conversion. Turnover rates were calculated by calculating the change in turnover number (the total amount of oxygenate product formed or amount of H_2O_2 consumed normalized by the total number of *active* M atoms used in a given reaction) as a function of time at differential conversion. In all reported data, the carbon balance closed within 98% and the standard uncertainty for measured reaction rates was <7%. Rates for the conversion of C_8H_8 and H_2O_2 were measured as functions of [H_2O_2] and [C_8H_8], and all reported results were obtained at differential conversion (i.e., <1% conversion of the limiting reagent for epoxide formation rates and <5% conversion of H_2O_2 for H_2O_2 consumption rates). Reported rates were measured in the absence of intra-pellet mass-transfer artifacts, as shown by satisfaction of the Madon–Boudart criterion[44] for Ti-BEA (i.e., the catalyst with the smallest pore diameter and largest rates; see SI, section S1.3) by performing reactions under identical conditions with Ti-BEA samples containing different metal loadings (SI, section S1.3). Over the loadings tested, epoxidation rates do not depend on the metal content, which shows that concentration gradients do not exist within the reactor or catalyst particles.

Styrene oxidation results in the formation of styrene oxide (C_8H_8O), phenylacetaldehyde, and benzaldehyde (C_7H_6O). Extrapolation of the selectivity for each of these products to the limit of zero C_8H_8 conversion shows that phenylacetaldehyde forms by isomerization of C_8H_8O over Lewis acid sites[45] and that both C_8H_8O and C_7H_6O form via primary reaction pathways (i.e., both give nonzero selectivities at nearly zero conversion). There are reports that benzaldehyde forms within the injection port of the gas chromatograph via oxidative decarboxylation of 1-phenyl-1,2-ethanediol.[46] Control experiments where a solution of 1-phenyl-1,2-ethanediol ("diol";

DOI: 10.1021/acscatal.7b03986
ACS Catal. 2018, 8, 2995–3010

Sigma-Aldrich, 97%) in CH_3CN (~0.01 M) was injected into the GC injection port show that <1% of the diol is converted to benzaldehyde under the GC method used. Additionally, C_7H_6O was not produced on any M-BEA materials and was produced with varying initial selectivities (30−50%) on all M-SiO_2 catalysts, which suggests that benzaldehyde forms catalytically and not within the GC. Here, the combined concentrations of C_8H_8O and phenylacetaldehyde are used to calculate initial rates for epoxidation reactions, which are used to develop the relationships between catalyst structure and function for alkene epoxidation.

2.4. Detection of Reactive Intermediates via In Situ UV−Vis and Raman Spectroscopy. In situ UV−vis spectroscopy was used to identify the intermediates formed upon H_2O_2 activation and confirm which among those intermediates are active for alkene epoxidation on M-BEA and M-SiO_2 materials.[10] Samples were pressed into 7 mm diameter pellets (~5 mg) and loaded into a custom built temperature-controlled UV−vis liquid flow cell. UV−vis spectra (100 scans, 600 ms integration time) were collected using a 45-degree diffuse reflection probe (Avantes, solarization-resistant fibers) coupled to a fiber-optic spectrometer (Avantes, AvaFast 2048) equipped with a compact deuterium-halogen light source (Avantes, AvaLight-DHc). Reactant and solvent solutions were introduced using a high-performance liquid chromatography pump (HPLC; Waters, 515). Background UV−vis spectra were obtained for each material by exposing the sample to a flowing CH_3CN solution (0.4 M H_2O, 1 cm^3 min^{-1}) at 313 K for 1 h. Samples were then activated with H_2O_2 by changing to a flowing solution of H_2O_2 in CH_3CN (0.1 M H_2O_2, 0.4 M H_2O, 1 cm^3 min^{-1}) at 313 K and continuing until the UV−vis spectra became constant (i.e., implying a steady-state coverage of surface intermediates). Samples were then flushed with pure CH_3CN (1 cm^3 min^{-1}) at 313 K for 10 min to remove residual H_2O_2 that had not been activated. Experiments to assign UV−vis features to specific surface intermediates (e.g., M-OOH or M-(η^2-O_2)) were performed by collecting UV−vis spectra at steady state while contacting M-BEA pellets with a solution of NH_4OH (Macron Chemicals, 28−30%; 0.01 M NH_4OH, 0.1 M H_2O_2, 0.4 M H_2O in CH_3CN, 313 K) and HCl (Ricca, 10 M; 0.01 M HCl, 0.1 M H_2O_2, 0.4 M H_2O in CH_3CN, 313 K) to shift the equilibrium between M-OOH and M-(η^2-O_2) intermediates (see section 3.1).

The reactivities of the surface intermediates observed in the UV−vis spectra were determined by continuously acquiring UV−vis spectra as a function of time while flowing a solution of cyclohexene (C_6H_{10}; Sigma-Aldrich, 99%) in CH_3CN (0.1 M C_6H_{10}, 0.4 M H_2O, 1 cm^3 min^{-1}) over H_2O_2-activated M-BEA and M-SiO_2 catalysts. Cyclohexene was used for these experiments to avoid complexities related to the secondary reactions that occur during styrene epoxidation. Specifically, the epoxidation of C_8H_8 resulted in the parallel reaction pathway that produced benzaldehyde on M-SiO_2 (see above), which prohibits detection of the reactive intermediate implicated in alkene epoxidation on M-SiO_2 materials. Rate constants for the consumption of these surface species via epoxidation and isomerization reaction were calculated by mathematically modeling the rates of peak attenuation (SI, section S2). Notably, independent experiments showed that the UV−vis absorbance features for H_2O_2-activated materials do not change or attenuate (within a period of 2 h) under a flowing stream of either CH_3CN (0.4 M H_2O, 1 cm^3 min^{-1}) or pure H_2O (1 cm^3 min^{-1}) at 313 K. Processes for peak smoothing, background subtraction, and peak fitting are described in the SI, section S2.

In situ Raman spectra were collected on a Raman microscopy (Renishaw, inVia) equipped with a 442 nm laser (Kimmon, IK3). Samples were pressed into 7 mm diameter pellets and were loaded into a custom Raman flow cell with a quartz window for spectral acquisition. Spectra were obtained using a long 50× objective with line-scan mode (~25 μm^2) and a laser power of 90 mW with 0.1 s acquisition times (300 co-averaged spectra). Reaction solutions were introduced via a HPLC pump and steady-state conditions were reached (i.e., where the spectra were unchanging with time) before acquiring spectra. Titanium oxysulfate (50 μL; Sigma, in 27−31% H_2SO_4) was combined with 1 μL of H_2O_2 (30% in H_2O) and was used to produce Ti(η^2-O_2)SO_4 for use as a reference compound.[47]

3. RESULTS AND DISCUSSION

3.1. Intermediates Formed upon Activation of H_2O_2. Figure 2 shows the UV−vis spectra of H_2O_2-activated M-BEA and M-SiO_2 materials acquired in situ (0.1 M H_2O_2, 0.4 M H_2O, in CH_3CN, 1 cm^3 min^{-1}). In all cases, UV−vis spectra possess two overlapping absorbance features, whose intensities are assumed to be proportional to the surface coverage of each UV−vis-active species. Previous reports from our laboratory mistakenly assigned the higher wavelength feature to hydroperoxide/peroxide (M-OOH/(η^2-O_2)) intermediates and the lower wavelength feature to the superoxide (M-$(O_2)^{-\bullet}$) moiety.[9,10] These assignments were based on published peak assignments that used a combination of in situ EPR and UV−vis spectroscopy to identify similar overlapping features on TS-1 to Ti-OOH and Ti-$(O_2)^{-\bullet}$,[19,48,49] and studies of amorphous Nb_2O_5 and Ta_2O_5 bulk oxides that assigned similar overlapping features on Nb and Ta contacted with H_2O_2 to the Nb-OOH (380 nm) and Nb-$(O_2)^{-\bullet}$ (320 nm) features.[50] Moreover, X-ray photoelectron spectra of H_2O_2-activated M-BEA (SI, section S1.3) show that Nb and Ta atoms reduce from M^{5+} to M^{4+};[9] however, it appears that the X-ray radiation caused photoreduction of the reactive complexes.[51] These data and literature precedents can lead to the incorrect conclusion that

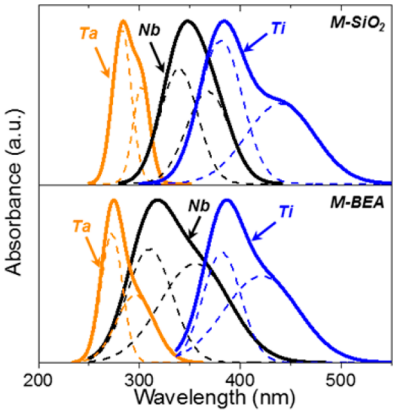

Figure 2. UV−vis spectra of H_2O_2-activated M-SiO_2 (top) and M-BEA (bottom) materials. Spectra were acquired in situ in flowing H_2O_2 in CH_3CN (0.1 M H_2O_2, 0.4 M H_2O, 1 cm^3 min^{-1}) at 313 K. Different colors indicate Ta (orange), Nb (black), and Ti (blue), and dashed lines represent deconvoluted Gaussian peaks for M-(η^2-O_2) and M-OOH species. Spectra for M-BEA materials are adapted from ref 10.

DOI: 10.1021/acscatal.7b03986
ACS Catal. 2018, 8, 2995−3010

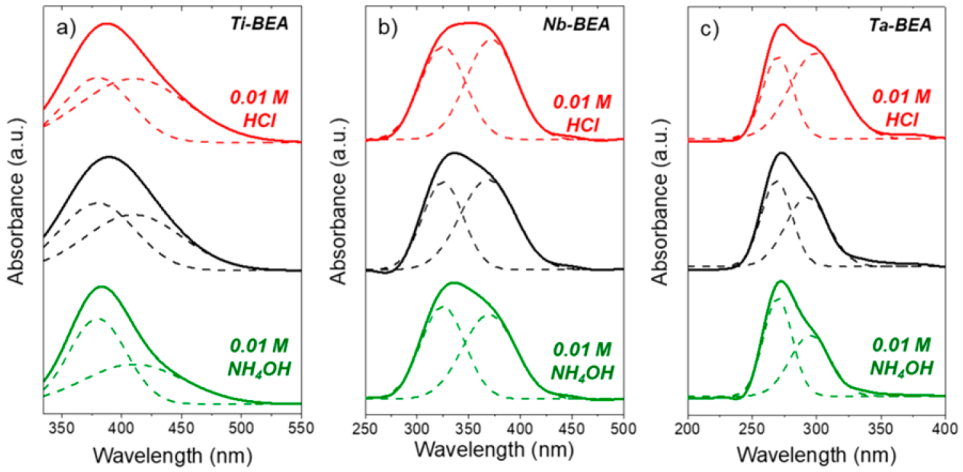

Figure 3. UV−vis spectra of H_2O_2-activated (a) Ti-BEA, (b), Nb-BEA, and (c) Ta-BEA. Spectra were acquired in situ in flowing H_2O_2 in CH_3CN (0.1 M H_2O_2, 0.4 M H_2O, 1 cm^3 min^{-1}; black), with HCl (0.01 M HCl, 0.1 M H_2O_2, 0.4 M H_2O, 1 cm^3 min^{-1}; red) or NH_4OH (0.01 M NH_4OH, 0.1 M H_2O_2, 0.4 M H_2O, 1 cm^3 min^{-1}; green) at 313 K. Dashed lines represent Gaussian peak fits for M-(η^2-O_2) and M-OOH species.

the UV−vis spectra contain features corresponding to M-$(O_2)^{-\bullet}$.

M-OOH intermediates are commonly invoked as the reactive intermediates on Ti-based heterogeneous catalysts for alkene epoxidation,[52−58] while both M-OOH and M-(η^2-O_2) have been observed spectroscopically on a various Ti, Nb, and Ta catalysts.[59−61] Yet much less is known about the identity of the reactive species involved in alkene epoxidation on Nb- and Ta-based heterogeneous catalysts, particularly in comparison to Ti-based catalysts (especially TS-1).

Figure 3 shows steady-state UV−vis spectra (0.1 M H_2O_2, 0.4 M H_2O in CH_3CN, 313 K) taken under basic (0.01 M NH_4OH), neutral, and acidic (0.01 M HCl) conditions for all M-BEA catalysts. For all Ti-, Nb-, and Ta-BEA catalysts, the ratio of the intensities of the absorbance feature at higher wavelengths to that of lower wavelength increases with the concentration of protons, which is determined by the water and NH_4OH or HCl present in the solvent. This suggests that the chemical species that is responsible for the UV−vis feature at higher wavelengths possesses an acidic proton and can be reversibly deprotonated to form a chemical species responsible for the lower wavelength feature. Scheme 1 shows that M-OOH forms M-(η^2-O_2) via reversible deprotonation, and the equilibrium between the two depends on the concentration of protons in the solvent.[54,55] Figure S10a shows Raman spectra collected in situ on Ti-BEA taken under identical neutral (0.1 M H_2O_2, 0.4 M H_2O, in CH_3Cl, 313 K), basic (0.01 M NH_4OH), and acidic (0.01 M HCl) solutions as those used in Figure 3. The Raman features at 491 and 750 cm^{-1} correspond to vibrations of the zeolite framework (e.g., O atom vibration perpendicular to M-O-M moieties).[62] The Raman feature at 621 cm^{-1} is well-known to correspond to ν(Ti−O_2) of Ti-(η^2-O_2).[53,54] The peak area of this 621 cm^{-1} feature increases upon adding NH_4OH and decreases upon adding HCl, which qualitatively corroborates the phenomena observed in Figure 3. Figure S10b shows the peak area of the 380 nm UV−vis feature correlates to the peak area of the 621 cm^{-1} Raman feature of Ti-(η^2-O_2), which shows that these two features correspond to the same species. In addition, both UV−vis and Raman show the changes in the peak areas are fully reversible (Figure S11), which demonstrates that these changes reflect the interconversion of these reactive intermediates and not their consumption by reaction with NH_4OH or HCl. These in situ UV−vis and Raman spectra of H_2O_2 activated catalysts together with reports of Tilley and co-workers[54] and Ivanchikova et al.[63] show that the higher wavelength species must be a M-OOH intermediate and the lower wavelength species should be a M-(η^2-O_2) on each M-BEA and M-SiO_2 catalyst.

Scheme 1. Consumption and Interconversion of M-OOH and M-(η^2-O_2) Species upon Reaction with C_6H_{10} on Group 4 Metals

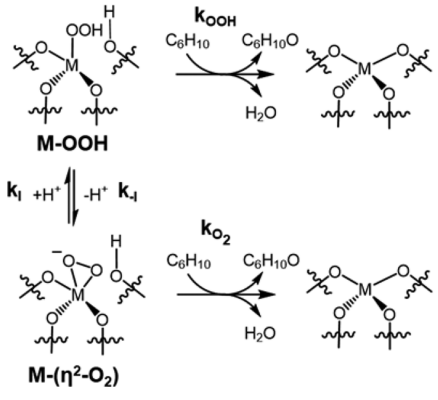

Notably, the flow of deionized H_2O or CH_3CN (1 cm^3 min^{-1}, 313 K) over H_2O_2-activated samples does not attenuate the UV−vis absorbance features during a period of 2 h on any of the M-BEA or M-SiO_2 samples, which suggests that H_2O_2 is activated irreversibly to form the M-(η^2-O_2) and M-OOH intermediates on these materials. Additionally, the similarities between the absorbance features (i.e., Figure 2) suggest that changing the type of silica support (i.e., M-BEA versus M-SiO_2) does not greatly affect the electronic properties or identity of the M-OOH and M-(η^2-O_2) species formed upon H_2O_2 activation.

In summary, these in situ UV−vis and Raman spectra strongly suggest that M-OOH (higher wavelength) and M-(η^2-O_2) (lower wavelength) species form irreversibly upon activation of H_2O_2 in CH_3CN, and that these species are plausible surface intermediates for alkene epoxidation.

3.2. Identification of Intermediates Responsible for Alkene Epoxidation. The identification of the exact active

DOI: 10.1021/acscatal.7b03986
ACS Catal. 2018, 8, 2995−3010

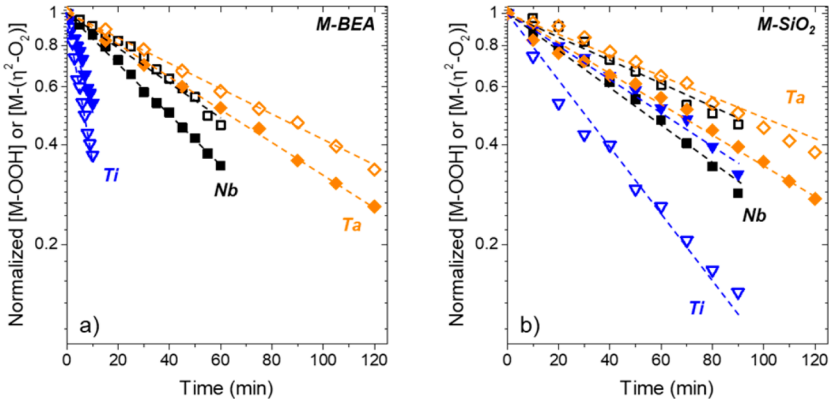

Figure 4. Change in the normalized surface coverages of M-OOH (open symbols) and M-(η^2-O_2) (closed symbols) as a function of time over (a) M-BEA and (b) M-SiO_2 materials. UV−vis spectra were obtained in situ upon contacting H_2O_2-activated materials with a solution of C_6H_{10} (0.1 M, 0.4 M H_2O, in CH_3CN, 1 cm^3 min^{-1}) at 313 K. Dashed lines represent fits to differential equations associated with Scheme 1 (see also SI, section S2). Symbols and colors represent Ti (blue ▼), Nb (black ■), and Ta (orange ◆) materials. M-BEA data are adapted from ref 10. Note that the vertical axes are log scale.

intermediate for alkene epoxidation among these M-BEA and M-SiO_2 materials is necessary in order to relate electronic structure of the reactive intermediates to epoxidation rates and selectivities. Figure 4 shows that the normalized intensities of the UV−vis absorbance features for M-OOH and M-(η^2-O_2) intermediates attenuate exponentially with time upon contact with a flowing solution containing cyclohexene (C_6H_{10}; 0.1 M, 0.4 M H_2O, in CH_3CN, 313 K). Differences in the rate of attenuation for individual UV−vis absorbance features indicate that specific intermediates are more reactive than others on each catalyst. For example, on Ti-BEA and Ti-SiO_2, the UV−vis features corresponding to Ti-OOH attenuate at a greater rate than those for Ti-(η^2-O_2), whereas the opposite trend is observed on Nb- and Ta-based catalysts.

Scheme 1 shows that H_2O_2 activates on M-BEA and M-SiO_2 materials to form a pool of M-OOH and M-(η^2-O_2) intermediates which then either interconvert or react with alkenes to yield epoxides and to regenerate the active site. The interconversion of these two species (k_I and k_{-I}) must be accounted for in order to accurately estimate the values of the rate constants for the consumption of M-OOH (k_{OOH}) and M-(η^2-O_2) (k_{O_2}) species by reaction with cyclohexene. The relationship between k_I and k_{-I} are constrained by the equilibrium coefficient (K_I; i.e., ratio of k_I to k_{-I}) that represents the ratio of M-OOH to M-(η^2-O_2) species under reaction conditions. (SI, section S2.3, outlines the procedure for estimating K_I on the different M-BEA materials.)

Table 2 shows the ratio of the rate constants for the reaction between M-OOH with C_6H_{10} to M-(η^2-O_2) with C_6H_{10} on all materials that are calculated by mathematically modeling the rate expressions derived from the mechanism in Scheme 1 (SI, section S2) and numerically determining the rate constants from the consumption of the species detected via in situ UV−vis (Figure 4). The differences between the rate constants for epoxidation by M-OOH and M-(η^2-O_2) intermediates reveal distinct periodic trends in reactivity.[10] Comparison of the ratio of calculated rate constants for M-OOH to M-(η^2-O_2) consumption on Ti materials show that the rate constant for Ti-OOH to epoxidize cyclohexene is greater than that for epoxidation by M-(η^2-O_2) (i.e., $k_{OOH} > k_{O_2}$), while the opposite is true for reactions on Nb and Ta catalysts (i.e., $k_{O_2} > k_{OOH}$). The difference between values of k_{OOH} and k_{O_2} on M-BEA and M-SiO_2 materials suggests that the active intermediate on Ti catalysts is Ti-OOH species, while Nb and Ta materials react through Nb-(η^2-O_2) and Ta-(η^2-O_2) complexes, respectively. The implication of these specific reactive intermediates on these materials was tested also by a complementary and independent method, described next.

Table 2. Ratio of the Rate Constants for the Consumption of M-OOH to That of M-(η^2-O_2) by Reaction with C_6H_{10} and *Z*:*E* (*cis*:*trans*) Product Ratios from the Epoxidation of *Z*-Stilbene (0.003 M *Z*-Stilbene, 0.005 M H_2O_2, in CH_3CN, 313 K)

sample	k_{OOH}:k_{O_2}	*Z*:*E* ratio
Ti-BEA	1.7	9.2 ± 0.3
Nb-BEA	0.6	1.0 ± 0.1
Ta-BEA	0.6	1.0 ± 0.1
Ti-SiO_2	11.1	10.1 ± 0.4
Nb-SiO_2	0.4	0.9 ± 0.1
Ta-SiO_2	0.5	0.9 ± 0.1

Analysis of the isomeric distribution of epoxide products formed by the reaction of *Z*-stilbene with H_2O_2 on M-BEA and M-SiO_2 catalysts (0.003 M *Z*-stilbene, 0.005 M H_2O_2, in CH_3CN, 313 K) can provide direct evidence for the identity of the reactive surface species (i.e., the "radical clock" technique).[64] Epoxidations of alkenes that involve M-OOH species proceed through a concerted O atom transfer step that retains the stereochemistry of the alkene reactant (i.e., through a "butterfly" transition state or Prilezhaev-type mechanism).[65−67] Alternatively, epoxidations that occur via M-(η^2-O_2) intermediates must react through a multi-step mechanism that involves the stepwise formation of the two C−O bonds that allows for rotation about the C−C bond to form the *E*-isomer. Examples of such mechanisms include those postulated for the stepwise formation of oxirane rings on homogeneous Mo complexes (later disproven)[68] and a biradical mechanism for homogeneous vanadium complexes.[69,70] Either mechanism could reproduce the mixture of isomers observed to form on the group 5 M-BEA and M-SiO_2 catalysts. Table 2 shows that Ti catalysts preferentially form *Z*-stilbene oxide, while Nb and Ta materials give nearly equimolar distributions of *Z*- and *E*-stilbene oxide products. Consequently, these selectivities indicate that epoxidations occur primarily through Ti-OOH

DOI: 10.1021/acscatal.7b03986
ACS Catal. 2018, 8, 2995−3010

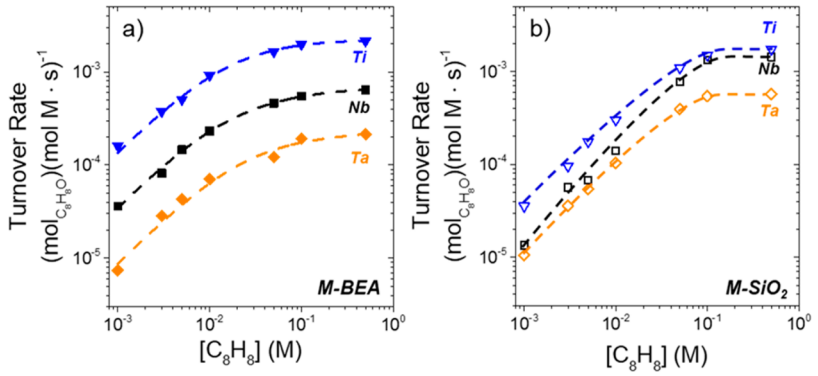

Figure 5. Turnover rates for the formation of styrene oxide via primary reaction pathways as a function of $[C_8H_8]$ for (a) M-BEA (closed symbols), including Ti-BEA (blue ▼, 0.01 M H_2O_2), Nb-BEA (black ■, 1 mM H_2O_2), and Ta-BEA (orange ◆, 1 mM H_2O_2) and (b) M-SiO_2 (open symbols), including Ti-SiO_2 (blue ▼, 0.01 M H_2O_2), Nb-SiO_2 (black ■, 0.01 M H_2O_2), and Ta-SiO_2 (orange ◆, 0.01 M H_2O_2) in CH_3CN at 313 K. Dashed lines are intended to guide the eye.

Scheme 2. Proposed Elementary Steps for C_8H_8 Epoxidation and H_2O_2 Decomposition over M-BEA and M-SiO_2 Catalysts[a]

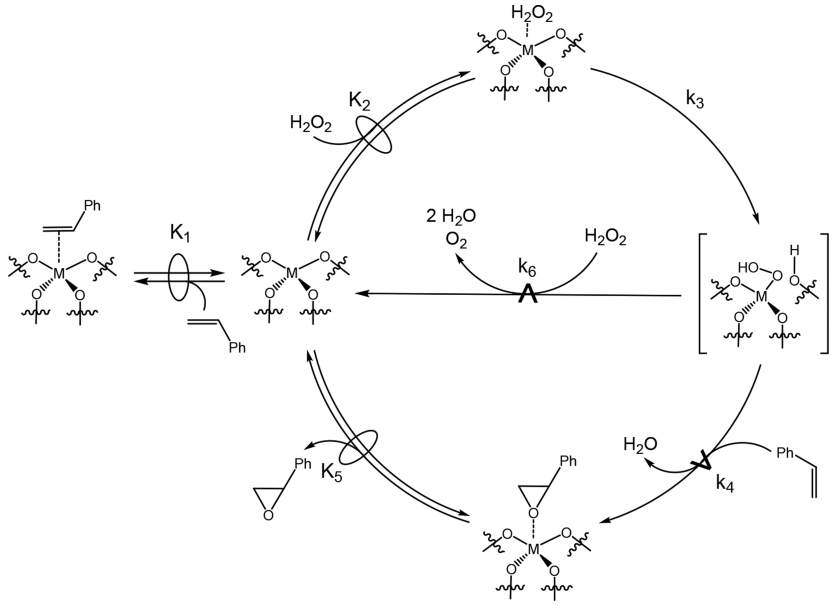

[a]For brevity, only group 4 catalysts (i.e., Ti) are shown. The oval superimposed over the equilibrium arrows represents a quasi-equilibrated step, while the carat (^) superimposed over the reaction arrow represents a kinetically relevant step. The depictions of M-OOH and adsorbed C_8H_8, H_2O_2, and C_8H_8O are meant to represent different types of surface species rather than suggest a specific type of coordination to the active catalytic site. Scheme S1 shows an analogous proposed set of elementary steps for group 5 (i.e., Nb and Ta) catalysts. The M-OOH intermediates drawn are intended to represent the pool of M-OOH and M-(η^2-O_2) species that are present as shown by UV−vis (Figure 2).

on Ti-BEA and Ti-SiO_2 and via Nb-(η^2-O_2) and Ta-(η^2-O_2) on the Nb and Ta catalysts, which are consistent with the interpretation of the in situ UV−vis measurements (Figure 4). Previous studies have shown that the microporous nature of the *BEA framework does not inhibit the diffusion of *Z*-stilbene or influence the preference for *Z*- or *E*-isomer formation,[10] which suggests also that the larger-pore SiO_2 supports do not influence the distribution among these epoxide products.

In summary, the independent estimates for the values of rate constants for specific elementary steps (Scheme 1) derived from the in situ UV−vis experiments (Figure 4) and the observed isomeric product distributions from reactions of *Z*-stilbene with H_2O_2 (Table 2) both indicate that all Ti-based materials in this study epoxidize alkenes through the Ti-OOH intermediate, while Nb- and Ta-based catalysts react through M-(η^2-O_2) species. Notably, the difference in coordination environment (i.e., metal atoms incorporated into the *BEA framework compared to those grafted onto mesoporous SiO_2) does not significantly affect the electronic structure (Figure 2) of the intermediates formed upon H_2O_2 activation.

3.3. Mechanistic Interpretations of Styrene Epoxidation Rates. Figure 5 shows turnover rates for the formation of styrene oxide (C_8H_8O) via primary reaction pathways as a function of $[C_8H_8]$ (0.001−0.5 M) over M-BEA (Figure 5a) and M-SiO_2 (Figure 5b) catalysts at constant $[H_2O_2]$ and temperature (313 K). For all materials, rates of C_8H_8O formation increase linearly with $[C_8H_8]$ and are independent of $[H_2O_2]$ (Figure S12a) and $[H_2O]$ (Figure S12c) at the lower values of $[C_8H_8]$ (<0.01 M C_8H_8), which suggests that surfaces are saturated with a H_2O_2-derived species. As the concentration of $[C_8H_8]$ increases (>0.05 M C_8H_8), the rate of C_8H_8O formation eventually becomes independent of $[C_8H_8]$ and proportional to $[H_2O_2]$ (Figure S12b). These concomitant changes in the dependence of the reaction rate on $[C_8H_8]$ and

DOI: 10.1021/acscatal.7b03986
ACS Catal. 2018, 8, 2995−3010

$[H_2O_2]$ suggest that the identity of the most abundant reactive intermediate (MARI) changes from a H_2O_2-derived species to one originating from C_8H_8. Scheme 2 depicts a series of elementary steps that account for the measured effects of $[C_8H_8]$ (Figure 5) and $[H_2O_2]$ (Figure S9) on the rates of C_8H_8 epoxidation. The catalytic cycle involves the quasi-equilibrated adsorption of C_8H_8 (step 1) and H_2O_2 (step 2), followed by the irreversible activation of H_2O_2 (step 3) to form a pool of M-OOH and M-(η^2-O_2) intermediates, which are collectively denoted as "M-(O_2)" for the subsequent development of rate expressions. The active M-(O_2) intermediates react either with C_8H_8 to form the epoxide (C_8H_8O, step 4) or with H_2O_2 (step 6) to decompose nonproductively. The C_8H_8O product subsequently desorbs in a quasi-equilibrated manner (step 5). C_8H_8O formation rates represent the kinetically relevant reaction of M-(O_2) with C_8H_8,

$$r_E = k_4[\text{M-}(O_2)][C_8H_8] \quad (1)$$

where r_E is the rate of C_8H_8O formation, [M-(O_2)] is the number of the reactive M-OOH complexes (for Ti) or M-(η^2-O_2) species (for Nb and Ta), and k_x is the rate constant for step x in Scheme 2. The application of the pseudo-steady-state hypothesis on the M-(O_2) intermediates, in conjunction with a site balance to account for all possible surface intermediates allows eq 1 to be restated as

$$\frac{r_E}{[L]} = \frac{\frac{k_3k_4K_2[H_2O_2][C_8H_8]}{k_4[C_8H_8] + k_6[H_2O_2]}}{\beta} \quad (2)$$

where [L] is the total number of *active* metal atoms present during the reaction, K_y is the equilibrium constant for step y, and β describes the summation of the numbers of all potential surface intermediates,

$$\beta = 1 + K_1[C_8H_8] + K_2[H_2O_2] + \frac{k_3K_2[H_2O_2]}{k_4[C_8H_8] + k_6[H_2O_2]} + K_5[C_8H_8O] \quad (3)$$

where the five terms in eq 3 correspond (in series) to catalytic sites occupied by CH_3CN (i.e., the reaction solvent), C_8H_8, H_2O_2, M-(O_2), or C_8H_8O (or phenylacetaldehyde), respectively. The complete derivation of the rate expression (eq 2) is shown in the SI, section S3.1.

Equation 2 reproduces the observed effects of $[C_8H_{10}]$ (Figure 5) and $[H_2O_2]$ (Figure S12) on epoxidation turnover rates. At low ratios of $[C_8H_8]$ to $[H_2O_2]$ (e.g., <5 on M-SiO_2 materials), M-(O_2) species are the MARI and eq 2 simplifies to the form

$$\frac{r_E}{[L]} = k_4[C_8H_8] \quad (4)$$

which is quantitatively consistent with turnover rates for styrene epoxidation that increase linearly with $[C_8H_8]$ (Figure 5) and do not depend on $[H_2O_2]$ (Figure S12a). Similarly, at higher $[C_8H_8]$ (e.g., >0.1 M) the reaction products (e.g., C_8H_8O or phenylacetaldehyde) become the MARI as indicated by epoxidation rates that are independent of $[C_8H_8]$ (Figure 5) and proportional to $[H_2O_2]$ (Figure S12b). In this limit, the rate of epoxidation is much greater than the rate of H_2O_2 decomposition (i.e., $k_4[C_8H_8] \gg k_6[H_2O_2]$; Table S4), which simplifies eq 2 to yield

$$\frac{r_E}{[L]} = \frac{k_3K_2[H_2O_2]}{k_6K_5[C_8H_8O]} \quad (5)$$

Equation 5 matches the ways in which r_E changes with variations in $[C_8H_8]$ and $[H_2O_2]$ at high $[C_8H_8]$. Notably, the dependence of styrene epoxidation rates on $[C_8H_8]$ and $[H_2O_2]$ resemble the changes in epoxidation turnover rates during cyclohexene epoxidation on M-BEA materials previously reported to occur through a perfectly analogous set of elementary steps.[9,10]

Equitable comparisons of turnover rates and selectivities require that the reaction conditions result in comparable MARIs (e.g., M-(O_2) across all M-BEA and M-SiO_2 materials. Figure 6 shows that rates and selectivities for C_8H_8 epoxidation

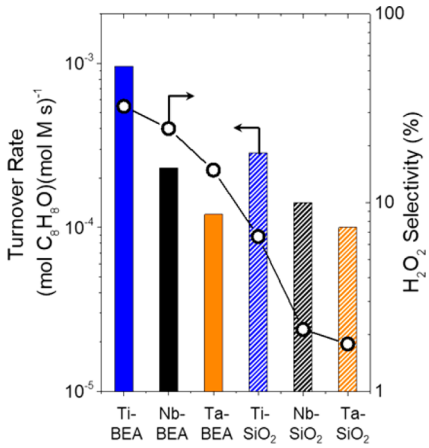

Figure 6. Turnover rates for the epoxidation of C_8H_8 (M-BEA, solid bars; M-SiO_2, striped bars; 0.01 M C_8H_8, 5 mM H_2O_2, 313 K) and H_2O_2 selectivities (calculated as the ratio of the rate of C_8H_8 epoxidation to total H_2O_2 consumption; ○).

differ significantly among the M-BEA and M-SiO_2 catalysts at standard conditions that result in M-(O_2) MARI for all materials (0.01 M C_8H_8, 5 mM H_2O_2, 313 K). For example, epoxidation turnover rates on Ti-BEA are ~10 times greater than those for Ta-BEA. In addition, H_2O_2 selectivities vary by a factor of 30 among these catalysts. Overall, epoxidation rates and selectivities are systematically greater for M-BEA materials than for the M-SiO_2 counterparts (e.g., rates and selectivities for Ti-BEA are greater than those on Ti-SiO_2 by factors of 7 and 5, respectively).

The underlying reasons for these large differences in rates and selectivities between Ti, Nb, and Ta atoms coordinated to the *BEA framework and those grafted to mesoporous SiO_2 must be related to physical differences between the two forms of silica supports. Specifically, these differences do not arise from changes in the identity of the reactive intermediates (section 3.2), which are constant for a given metal atom nor from the reaction mechanisms, which are indistinguishable among the catalysts described here. Therefore, the differences among the performance of the catalysts must be caused by consequential differences in the apparent activation barriers for C_8H_8 epoxidation and H_2O_2 decomposition, respectively, that are associated with the crystallographic or morphological differences between the crystalline *BEA framework and the amorphous mesoporous silica support.

3.4. Influence of Metal Identity on Activation Barriers.

Transition-state theory (TST) provides a theoretical founda-

DOI: 10.1021/acscatal.7b03986
ACS Catal. 2018, 8, 2995−3010

tion to quantify the stabilities of the transition states for C_8H_8 epoxidation (eq 6) and for H_2O_2 decomposition (eq 7) relative

$$M-(O_2)+C_8H_8 \rightleftharpoons M-(O_2)-C_8H_8^{\ddagger} \quad (6)$$

$$M-(O_2)+H_2O_2 \rightleftharpoons M-(O_2)-H_2O_2^{\ddagger} \quad (7)$$

to a known reference state in the catalytic cycle (e.g., the state in which the MARI occupies the active site; see SI, section S3.2).[71] In order to make equitable comparisons between M-BEA and M-SiO_2 catalysts, activation barriers must be measured from comparable MARI. Application of TST assumes that the elementary step immediately preceding the transition state (e.g., M-(O_2) and fluid-phase C_8H_8 or H_2O_2) and the transition state are in equilibrium,[71] where M-(O_2)-$C_8H_8^{\ddagger}$ and M-(O_2)-$H_2O_2^{\ddagger}$ represent the epoxidation and H_2O_2 decomposition transition states, respectively. Consequently, the apparent free energies of activation ($\Delta G^{\ddagger}$) represent the difference in the relative free energy between the transition state and reference states, as shown by

$$\Delta G^{\ddagger} = G^{\ddagger} - G_{M\text{-}(O_2)} - G_X \quad (8)$$

where $G^{\ddagger}$ is the free energy of the relevant transition state (i.e., for C_8H_8 epoxidation or H_2O_2 decomposition), $G_{M\text{-}(O_2)}$ is the free energy of the M-(O_2) reactive intermediates, and G_X is the free energy of fluid-phase C_8H_8 or H_2O_2. Equation 8 emphasizes the need to have a consistent MARI on all catalysts, in order to probe how differences in the identity of the transition metal atoms or type of silica support (i.e., M-BEA versus M-SiO_2) used influence activation barriers for epoxidation and H_2O_2 decomposition. Values of the activation enthalpies ($\Delta H^{\ddagger}$) and entropies ($\Delta S^{\ddagger}$) for reactions shown in eqs 6 and 7 are obtained by analysis of transition state equilibrium constants measured as functions of inverse temperature (SI, Figure S13 and section S3.2) using the Eyring equation.[71]

Table 3 shows activation enthalpies and entropies for both C_8H_8 epoxidation ($\Delta H^{\ddagger}_E$ and $\Delta S^{\ddagger}_E$) and H_2O_2 decomposition ($\Delta H^{\ddagger}_D$ and $\Delta S^{\ddagger}_D$) obtained at reaction conditions that result in a M-(O_2) MARI on each M-BEA and M-SiO_2 sample and in the absence of mass-transfer and diffusive limitations (SI, section S1.3). Table 3 shows that $\Delta H^{\ddagger}$ values increase in the order of Ti < Nb < Ta for a given type of catalyst (i.e., M-BEA or M-SiO_2), which is consistent with the differences in turnover rates in Figure 5 and in agreement with previous findings for cyclohexene epoxidation on M-BEA (M = Ti, Nb, Ta, Zr, and Hf) catalysts.[10] Values of $\Delta H^{\ddagger}_E$ for M-BEA materials are, on average, ~20 kJ mol^{-1} lower than the values for the corresponding M-SiO_2 catalysts (e.g., 9 ± 3 kJ mol^{-1} versus 30 ± 4 kJ mol^{-1} for Ti-BEA and Ti-SiO_2, respectively).

Values of $\Delta H^{\ddagger}_D$, however, do not depend on the identity of the support for a given metal atom (e.g., 45 ± 5 kJ mol^{-1} versus 42 ± 4 kJ mol^{-1} for Nb-BEA and Nb-SiO_2, respectively). Additionally, $\Delta S^{\ddagger}_E$ values do not change significantly within a given type of material (e.g., across M-SiO_2), within the uncertainty of measurements. $\Delta S^{\ddagger}_E$ values reflect the loss of translational entropy that arises from coordination of C_8H_8 to the active M-(O_2) species, which is not expected to depend on the identity of the metal. Notably, values of $\Delta S^{\ddagger}_E$ for M- BEA are ~50 J mol^{-1} K^{-1} more negative than M-SiO_2 (i.e., a greater entropic loss on M-BEA), which likely arises from the smaller pores of the *BEA framework (0.7 nm for *BEA versus 5.4 nm for SiO_2) confining the epoxidation transition state to a greater extent than SiO_2.

Interestingly, $\Delta S^{\ddagger}_D$ values do not change when the identity of the metal or the type of silica support (i.e., M-BEA and M-SiO_2) are changed, which suggests that neither the difference in transition metal identity nor change in pore diameter significantly influences the transition state for H_2O_2 decomposition.

Figure 7 shows that values of $\Delta H^{\ddagger}_E$ for C_8H_8 epoxidation correlate linearly with the enthalpies of adsorption for CD_3CN or pyridine (Table 1, section 2.2) coordinated to Lewis acid sites, which each provide a functional probe of the strength of Lewis acid sites among M-BEA and M-SiO_2 catalysts. These values (i.e., ΔH_{Py} and ΔH_{CD_3CN}) are *not* measurements of Lewis acid strength and *cannot* be used to compare properties of Lewis acid sites on M-BEA to those on M-SiO_2, because the

Table 3. Activation Enthalpies and Entropies for C_8H_8 Epoxidation ($\Delta H^{\ddagger}_E$ and $\Delta S^{\ddagger}_E$) and H_2O_2 Decomposition ($\Delta H^{\ddagger}_D$ and $\Delta S^{\ddagger}_D$) over M-BEA and M-SiO_2 Catalysts Measured on M-(O_2) Saturated Active Sites[a]

sample	$\Delta H^{\ddagger}_E$ (kJ mol^{-1})	$\Delta S^{\ddagger}_E$ (J mol^{-1} K^{-1})	$\Delta H^{\ddagger}_D$ (kJ mol^{-1})	$\Delta S^{\ddagger}_D$ (J mol^{-1} K^{-1})
Ti-BEA	9 ± 3	−200 ± 55	31 ± 10	−104 ± 40
Nb-BEA	39 ± 5	−150 ± 34	45 ± 5	−91 ± 30
Ta-BEA	50 ± 6	−130 ± 45	56 ± 5	−61 ± 25
Ti-SiO_2	30 ± 4	−90 ± 25	34 ± 5	−110 ± 25
Nb-SiO_2	57 ± 5	−75 ± 20	42 ± 4	−99 ± 18
Ta-SiO_2	71 ± 5	−68 ± 15	60 ± 5	−75 ± 20

[a]Reported values are calculated from transition state equilibrium constants for styrene epoxidation and H_2O_2 decomposition determined as functions of inverse temperature (SI, Figure S13 and section S3.2). $\Delta H^{\ddagger}_D$ and $\Delta S^{\ddagger}_D$ values for M-BEA are adapted from ref 10.

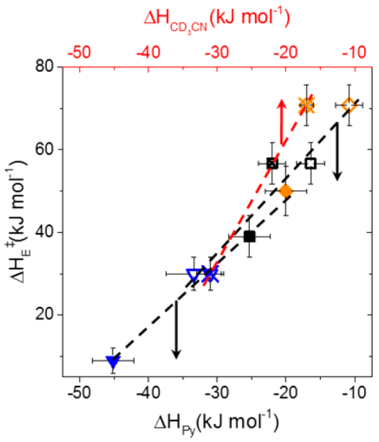

Figure 7. Comparisons between activation enthalpies for C_8H_8 epoxidation ($\Delta H^{\ddagger}_E$) and the enthalpies of adsorption for pyridine (ΔH_{Py}; solid and open symbols) or deuterated acetonitrile (ΔH_{CD_3CN}; symbols with cross (×) through them) bound to Lewis acid sites over M-BEA (solid and crossed symbols) or M-SiO_2 (open symbols) measured on a M-(O_2) saturated surface. Color symbols represent: Ti (blue ▼), Nb (black ■), and Ta (orange ◆). Dashed lines are intended to guide the eye.

DOI: 10.1021/acscatal.7b03986
ACS Catal. 2018, 8, 2995−3010

values of ΔH_{Py} and ΔH_{CD_3CN} also depend on dispersive interactions (i.e., van der Waals forces) between the adsorbates and the surfaces of the microporous *BEA or the mesoporous SiO_2. These results (i.e., linear correlations in Figure 7) resemble the linear relationships reported between the activation enthalpies cyclohexene epoxidation and ΔH_{CD_3CN} previously reported for M-BEA catalysts (M = Ti, Zr, Hf, Nb, and Ta),[10] for which the stabilization of cyclohexene epoxidation transition states by dispersive interactions was similar among all M-BEA.

The underlying causes of these observed trends (Figure 7) and the correlations shown for cyclohexene epoxidation[10] are nuanced and do not reflect a simple linear dependence on "Lewis acid strength", which cannot be readily measured. $\Delta H^{\ddagger}_{E}$ values correlate to the adsorption enthalpies for pyridine and CD_3CN coordinated to Lewis acid sites for these materials, but these correlations may be fortuitous. Rather, values of $\Delta H^{\ddagger}_{E}$ (and thus, epoxidation rates) depend on the electrophilicity of the reactive intermediates (M-(O_2)), which in turn are influenced by the tendency of the metal center to withdraw electron density from the −OOH or $-O_2^-$ moieties. Figure 7 suggests that pyridine and CD_3CN donate electrons to these Lewis acidic sites in ways that happen to be similar to the distribution of charge at the transition state for epoxidation, and as a result, a linear correlation exists.

UV−vis spectra of H_2O_2-activated catalysts provide direct and quantitative measures of the electronic structure of the reactive M-OOH and M-(η^2-O_2) complexes in the form of ligand-to-metal charge transfer band energies (LMCT $h\nu$). These LMCT $h\nu$ values reflect the tendency of the metal atoms to accept electrons from these moieties (i.e., another functional measure of the Lewis acid strength).[10] Figure 8a shows that

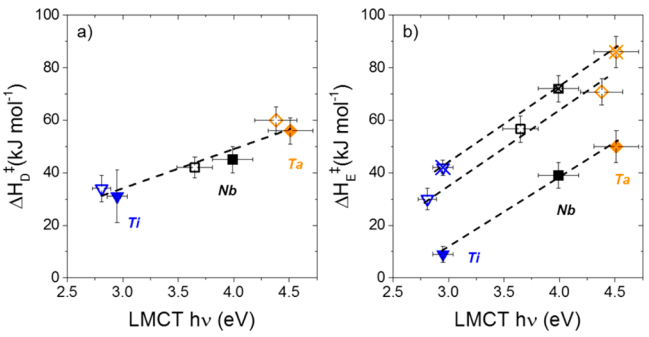

Figure 8. Activation enthalpies for (a) H_2O_2 decomposition ($\Delta H^{\ddagger}_{D}$; solid and open symbols for M-BEA and M-SiO_2, respectively) and (b) epoxidation of C_8H_8 ($\Delta H^{\ddagger}_{E}$; solid and open symbols for M-BEA and M-SiO_2, respectively) or C_6H_{10} (open symbols with a cross (×) for M-BEA) epoxidation measured on M-(O_2) saturated surfaces as a function of ligand-to-metal charge-transfer energy (LMCT $h\nu$) of the reactive intermediate identified via in situ UV−vis (section 3.1) and *Z*-stilbene epoxidation product distributions. Color symbols represent: Ti (blue ▼), Nb (black ■), and Ta (orange ♦). Dashed lines are intended to guide the eye. Values of $\Delta H^{\ddagger}_{E}$ for C_6H_{10} epoxidation on M-BEA materials are adapted from ref 10.

values of $\Delta H^{\ddagger}_{D}$ depend linearly on LMCT $h\nu$ for all materials, which strongly suggests that materials that possess more electrophilic M-OOH and M-(η^2-O_2) intermediates give greater rates for H_2O_2 decomposition. Similarly, Figure 8b demonstrates that values of $\Delta H^{\ddagger}_{E}$ for C_8H_8 and C_6H_{10} epoxidation over M-BEA and M-SiO_2 also depend linearly on the value of the LMCT $h\nu$, and moreover, the slopes for these dependencies are nearly equal on both M-BEA and M-SiO_2 catalysts. These comparisons suggest that more electrophilic M-OOH and M-(η^2-O_2) species are also more reactive for alkene epoxidation. However, $\Delta H^{\ddagger}_{E}$ depends more strongly on LMCT $h\nu$ in all cases (slope ∼28 kJ mol^{-1} eV^{-1}; Figure 8b) than does $\Delta H^{\ddagger}_{D}$ (slope ∼15 kJ mol^{-1} eV^{-1}; Figure 8a), which indicates that the selectivities for epoxidation also increase with the electrophilicity of the reactive M-OOH and M-(η^2-O_2) intermediates. The greater dependence of $\Delta H^{\ddagger}_{E}$ on LMCT $h\nu$ than $\Delta H^{\ddagger}_{D}$ may be attributed to the inherent instability of the peroxide (i.e., O−O) bond in H_2O_2, as the decomposition of H_2O_2 by reaction with M-OOH intermediates in Ti-SBA-15 has been proposed to occur through a homolytic pathway (i.e., that involves the cleaving of the HO−OH bond).[55] Finally, the correlation of $\Delta H^{\ddagger}_{E}$ for C_8H_8 epoxidation to the values of LMCT $h\nu$ (Figure 8b) show that $\Delta H^{\ddagger}_{E}$ are consistently ∼20 kJ mol^{-1} greater for M-SiO_2 catalysts in comparison to M-BEA materials with similar LMCT $h\nu$.

The clear correlations between $\Delta H^{\ddagger}$ and LMCT $h\nu$ values shown in Figure 8 are more relevant and meaningful than the correlations to ΔH_{Py} and ΔH_{CD_3CN} (Figure 7), because values of LMCT $h\nu$ report on the electronic structure of an intermediate directly involved in the kinetically relevant steps that dictate turnover rates and selectivities for epoxidations (Scheme 2, steps 4 and 6). Interpretation of the trends shown in Figure 8b reveal several important phenomena. First, the increasing rates and selectivities with decreasing LMCT $h\nu$ (i.e., more electrophilic M-OOH and M-(η^2-O_2) intermediates that are associated with lower-energy electronic transitions) suggests that these intermediates are electrophilic in nature, which results from the stronger electron-withdrawing nature of the Lewis acidic metal center. Second, the unchanging dependence of LMCT $h\nu$ on $\Delta H^{\ddagger}_{E}$ for both C_8H_8 and C_6H_{10} epoxidation suggests that there may be little, if any, benefit (i.e., changes in selectivities differing from the trend observed in Figure 8) to changing the identity of the metal for different alkene substrates. Third, the constant vertical offset in $\Delta H^{\ddagger}_{E}$ for C_8H_8 epoxidation of M-BEA and M-SiO_2, and lack thereof for $\Delta H^{\ddagger}_{D}$, suggests that the pore size of the *BEA framework relative to SiO_2 primarily influences the rates of epoxidation, but not H_2O_2 decomposition. Each of these observations and suggested descriptions is discussed in detail in the following sections.

The electrophilic nature of the M-OOH and M-(η^2-O_2) species and the unchanging trend in epoxidation rates for C_8H_8 and C_6H_{10} epoxidation on M-BEA can be probed further by measuring the changes in reactions rates that result from systematically changing the electronic structure of the C=C bond in styrene by incorporating different substituents at the *para*-position. Figure 9 shows that the ratio of the turnover rates for the epoxidation of *para*-substituted styrenes (x-C_8H_7, where x = -NO_2, -Br, -H, -Me, or -OMe) to C_8H_8 (R_x/R_H) decreases exponentially with increasing values of the *para* Hammett substituent constant (σ_{para}) on all M-BEA and M-SiO_2 catalysts at a standard set of conditions (3 mM x-C_8H_7, 0.01 M H_2O_2, in CH_3CN, 313 K). These data strongly suggest that epoxidation rates increase with the electron-donating ability of the *para* substituent among these reactants. Values of R_x/R_H depend similarly on σ_{para} for all M-BEA and M-SiO_2, and are fit using the Hammett equation,

DOI: 10.1021/acscatal.7b03986
ACS Catal. 2018, 8, 2995−3010

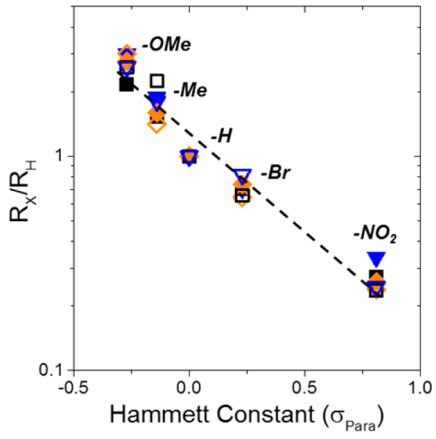

Figure 9. Ratio of the turnover rates for the epoxidation of *para*-substituted styrene (x-C_8H7; x = -NO_2, -Br, -H, -Me, or -OMe) to styrene (3 mM x-C_8H_8, 0.01 M H_2O_2, in CH_3CN, 313 K) as a function of the Hammett constant (i.e., a Hammett plot) on M-BEA (solid symbols) and M-SiO_2 (open symbols). Color symbols represent Ti (blue ▼), Nb (black ■), and Ta (orange ◆). The dashed line represents a fit of eq 9 to all data, which yields a reaction constant (ρ; Table S5 for all individual ρ values) of −0.9 ± 0.1.[72]

$$\log\left(\frac{k_x}{k_H}\right) = \sigma_{para}\rho \tag{9}$$

where k_x and k_H are the rate constants for x-C_8H_7 epoxidation and ρ is the reaction constant (calculated ρ values for all M-BEA and M-SiO_2 are in Table S4).

The turnover rates for x-C_8H_7 epoxidation (R_x) were used in place of k_x, because all reactions were run at equivalent conditions. The average value of ρ (calculated by averaging all ρ for each M-BEA and M-SiO_2 material; Table S5) is −0.9 ± 0.1, whose negative sign agrees with the loss of negative charge (i.e., reduction of M-OOH or M-(η^2-O_2) during epoxidation) that occurs during the 2-electron oxidation of x-C_8H_7 and shows that electrophilic intermediates possess lower activation barriers (i.e., higher rates) for the epoxidation of increasingly electron-rich C═C.[72] Further, the invariance of ρ (i.e., the similarity among values of ρ; Table S5) between all M-BEA and M-SiO_2 suggests that the rates of alkene epoxidation change similarly on all materials when the identity (and electronic properties) of the alkene is changed. This suggests that the chemoselectivity for alkene epoxidation (specifically for molecules with multiple C═C) may be independent of the type of metal atom used in these M-BEA or M-SiO_2 materials.

3.5. Influence of the Average Pore Diameter of the Catalyst on Activation Barriers. Scheme 3 shows changes in enthalpies that correspond to a set of hypothetical elementary steps for the epoxidation of styrene on M-BEA and M-SiO_2 catalysts that correspond to the proposed catalytic cycle (Scheme 2) and the prevalence of M-OOH and M-(η^2-O_2) species on the active sites at the conditions (i.e., the reference state) used to measure apparent $\Delta H^{\ddagger}_E$ values (i.e., $\Delta H^{\ddagger}_{App}$).[71,73] Briefly, styrene adsorbs from the fluid phase into the micro- or mesoporous environment near the active M-OOH or M-(η^2-O_2) complex, which corresponds to the enthalpy for adsorption into the porous environment (i.e., ΔH_{Ads}). Subsequently, adsorbed styrene and M-OOH or M-(η^2-O_2) combine to form the transition state for epoxidation and undergo an enthalpy change equal to the intrinsic activation enthalpy for the epoxidation reaction ($\Delta H^{\ddagger}_{Int}$).

Scheme 3. Changes in Enthalpies Due to the Intermediate Steps That Form the Transition State for C_8H_8 Epoxidation from a M-(O_2) Saturated Surface and Fluid-Phase C_8H_8[a]

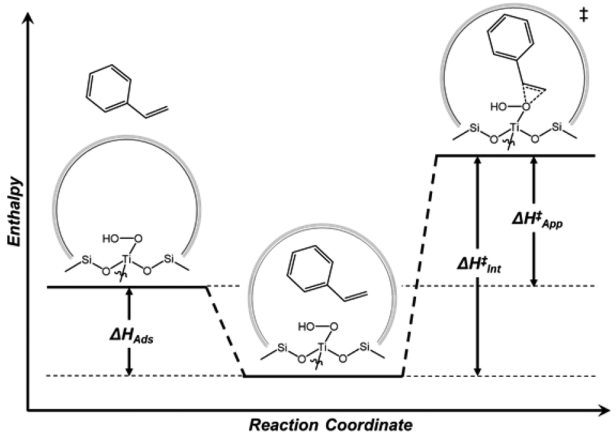

[a]Ti-OOH is shown to illustrate the relationship between $\Delta H^{\ddagger}_{App}$, ΔH_{Ads}, and $\Delta H^{\ddagger}_{Int}$ (see Scheme S2 for analogous scheme for group 5 catalysts). This thermochemical sequence for the epoxidation of C_8H_8 with a Ti-OOH reference state (i.e., Ti-OOH MASI) uses a transition-state theory formalism that involves the quasi-equilibrated adsorption of C_8H_8 into the pores of *BEA or SiO_2 and the kinetically relevant reaction of C_8H_8 with Ti-OOH.

Scheme 3 shows that $\Delta H^{\ddagger}_{App}$ can be related to the other two enthalpy differences as follows

$$\Delta H^{\ddagger}_{App} = \Delta H^{\ddagger}_{Int} - |\Delta H_{Ads}| \tag{10}$$

In this sequence (Scheme 3), both the ΔH_{Ads} into the porous voids and, by extension, $\Delta H^{\ddagger}_{App}$ depend on morphological properties of the catalyst (e.g., pore size) and the kinetic diameter of the alkene. Values for ΔH_{Ads} are measured directly by applying van't Hoff analysis to measurements of C_8H_8 uptake obtained at identical liquid-phase concentrations (0.03 mM for Si-BEA and 0.007 mM for SiO_2). These ΔH_{Ads} (35 ± 6 kJ mol^{-1} and 18 ± 3 kJ mol^{-1} for Si-BEA and SiO_2, respectively) are measured in liquid CH_3CN (the reaction solvent) to account for the displacement of CH_3CN from the vicinity of the active site. The values of $\Delta H^{\ddagger}_{Int}$ for each catalyst are calculated using eq 10 and measured values for ΔH_{Ads} and $\Delta H^{\ddagger}_{App}$.

Figure 10 shows that $\Delta H^{\ddagger}_{Int}$ for C_8H_8 epoxidation for all M-BEA and M-SiO_2 materials correlate linearly with the LMCT $h\nu$. Moreover, all $\Delta H^{\ddagger}_{Int}$ fall near a single line, which suggests that subtle differences between the coordination of these transition metal centers to crystalline *BEA or amorphous SiO_2 do not change the relationship between $\Delta H^{\ddagger}_{Int}$ and the electronic structure (i.e., LMCT $h\nu$) of the reactive M-OOH or M-(η^2-O_2) intermediates (section 3.1). These similarities seem to be a reasonable result of the nearly equivalent values for LMCT $h\nu$ for specific M-(O_2) complexes on *BEA and SiO_2 supports (i.e., LMCT $h\nu$ for Ti-BEA is not statistically different from that for Ti-SiO_2), suggested by the corresponding UV−vis spectra (section 3.1, Figure 2). Consequently, these data (Figure 10) suggest that the electronic structure and the intrinsic reactivity of these M-OOH and M-(η^2-O_2) complexes do not depend on the choice of siliceous support.

The combination of nearly equal values for $\Delta H^{\ddagger}_{Int}$ on a given transition metal in *BEA or SiO_2, the similar LMCT $h\nu$ for these same complexes, and the relationships depicted in

DOI: 10.1021/acscatal.7b03986
ACS Catal. 2018, 8, 2995−3010

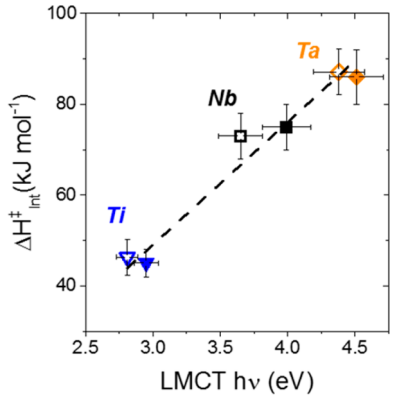

Figure 10. Intrinsic activation enthalpies ($\Delta H^{\ddagger}_{Int}$) for the epoxidation of C_8H_8 over M-BEA (closed symbols) and M-SiO_2 (open symbols) measured on a M-(O_2) saturated surface (Figure 8b) as a function of ligand-to-metal charge transfer energies (LMCT $h\nu$). Color symbols represent: Ti (blue ▼), Nb (black ■), and Ta (orange ◆). Dashed line represents a linear regression to all data.

Scheme 3 indicate that the differences in turnover rates, selectivities, and $\Delta H^{\ddagger}_{App}$ are consequences of differences in the values of ΔH_{Ads} for styrene within the pores of *BEA (−35 ± 6 kJ mol^{-1} in 0.7 nm siliceous pores)[74] and SiO_2 (−18 ± 3 kJ mol^{-1} in 5.4 nm siliceous pores). Thus, stronger, dispersive interactions within the smaller pores of *BEA preferentially stabilize the transition state for styrene epoxidation relative to that in SiO_2 (and also H_2O_2 decomposition transition states in both materials) and leads to $\Delta H^{\ddagger}_{E}$ values that are systematically ∼20 kJ mol^{-1} lower in M-BEA than on M-SiO_2 catalysts (Figure 8b). Notably, values of $\Delta H^{\ddagger}_{D}$ (Figure 8a) do not depend on the pore size of the catalyst, which suggests that the same dispersive interactions that preferentially stabilize the transition state for C_8H_8 epoxidation do not affect H_2O_2 decomposition. H_2O_2 has a Stokes diameter (∼0.24 nm)[75] that is significantly smaller than the diameter of the pores within *BEA (∼0.7 nm) or SiO_2 (5.4 nm), which suggests that H_2O_2 cannot be stabilized as significantly as styrene by interactions with the pore walls at the transition state for decomposition. Previous studies investigating the oxidation of alkanes and alkenes on TS-1 and Ti-silicate (TiO_2−SiO_2) have shown that TS-1 possesses significantly higher rates and selectivities for 1-hexene epoxidation and cyclohexanone ammoxidation using aqueous H_2O_2.[64,76,77] These reports attributed the large differences in reactivity (i.e., a 30-fold increase in rates and 10-fold increase in selectivities for 1-hexene epoxidation) to a smaller number of Ti active sites that are available for reaction in TiO_2−SiO_2 than TS-1.[64] However, it seems likely that the differences may have arisen from greater heats of adsorption of 1-hexene (and likely cyclohexanone) in the MFI framework relative to mesoporous TiO_2−SiO_2 which results in a concomitant decrease in the apparent activation enthalpies for epoxidation[64] (and ammoxidation).[76,77] Consequently, these data and interpretations reveal two orthogonal design criteria for alkene epoxidation catalysts. First, the design of materials with greater electron affinities (i.e., stronger Lewis acids) will result in more electrophilic M-(O_2) intermediates that possess both increased rates and selectivities for alkene epoxidation. Second, the pore environment (i.e., pore diameter, and likely the hydrophobic/hydrophilic character)[78−81] surrounding the active sites can be selected to maximize dispersive interactions with the desired alkene and increase the transition state stabilization for epoxidation to confer both greater rates and selectivities. Ongoing studies in our group seek to understand the effects of silanol density (and how this relates to hydrophilicity) on the rates and selectivities of alkene epoxidation within similar materials.

4. CONCLUSIONS

In situ UV−vis spectroscopy reveals that Ti, Nb, and Ta metal atoms incorporated into the *BEA zeolite framework or atomically grafted onto mesoporous SiO_2 irreversibly activate H_2O_2 to form pools of hydroperoxide and peroxide. The isomeric product distributions from reactions with *Z*-stilbene, in conjunction with time-resolved UV−vis spectra of the reaction of H_2O_2-activated materials with cyclohexene, reveal that Ti-materials primarily react through the Ti-OOH intermediate, while Nb- and Ta- catalysts react through the M-(η^2-O_2) species. This suggests that changing the type of silica support from the *BEA framework to mesoporous SiO_2 does not significantly influence the identity or electronic properties of the reactive intermediates for epoxidation by these group IV and V catalysts. Moreover, the dependence of styrene oxide formation rates on reactant (i.e., C_8H_8 and H_2O_2) concentrations show that all M-BEA and M-SiO_2 react through a nearly identical mechanism. All catalysts first adsorb H_2O_2, followed by irreversible activation to form a pool of M-OOH and M-(η^2-O_2) intermediates, which then react with styrene or H_2O_2 to form the corresponding epoxide or decomposition products, respectively. Correlation of activation enthalpies for C_8H_8 epoxidation and H_2O_2 decomposition, on all M-BEA and M-SiO_2 catalysts, to the ligand-to-metal charge transfer band energies of the reactive intermediates show more electrophilic M-OOH or M-(η^2-O_2) species are both *more reactive and selective* for alkene epoxidation. Hammett analysis for the epoxidation of *para*-substituted styrene shows that all M-BEA and M-SiO_2 possess similar chemoselectivities for the epoxidation of alkenes with varying electronic properties. The rates and selectivities of C_8H_8 epoxidation are systematically higher on M-BEA than M-SiO_2 materials, which arise from increased dispersive interactions of the transition state for epoxidation with the walls of *BEA relative to that of SiO_2. This work reveals two discrete design criteria for epoxidation catalysts—the electron affinity of the catalytic site that affects the electrophilicity of the active complex, where more electrophilic intermediates are more active and selective for epoxidation, and the size of the surrounding pore, which can selectively stabilize transition states for epoxidation relative to H_2O_2 decomposition.

■ ASSOCIATED CONTENT

Supporting Information

The Supporting Information is available free of charge on the ACS Publications website at DOI: 10.1021/acscatal.7b03986.

Characterization data, M-BEA active-site titrations, X-ray photoelectron data, in situ UV−vis data analysis, rate expression derivation, activation enthalpy and entropy calculations, and Hammett reaction constants, including Schemes S1 and S2, Tables S1−S5, and Figures S1−S13 (PDF)

■ AUTHOR INFORMATION

Corresponding Author

*E-mail: dwflhrty@illinois.edu.

DOI: 10.1021/acscatal.7b03986
ACS Catal. 2018, 8, 2995−3010

ORCID

Daniel T. Bregante: 0000-0003-2157-1286
Nicholas E. Thornburg: 0000-0002-4680-2733
Justin M. Notestein: 0000-0003-1780-7356
David W. Flaherty: 0000-0002-0567-8481

Present Address

[§]N.E.T.: National Bioenergy Center, National Renewable Energy Laboratory, 15013 Denver West Parkway, Golden, CO 80401, United States

Notes

The authors declare no competing financial interest.

■ ACKNOWLEDGMENTS

We thank Ms. Megan Witzke for XPS sample preparation and helpful comments, Ms. Zeynep Ayla for proofreading of the manuscript and helpful discussions, and Dr. Damien Guironnet for use of laboratory equipment to synthesize Ti-BEA. D.T.B. was supported by the Department of Defense (DoD) through the National Defense Science & Engineering Graduate Fellowship (NDSEG) Program. N.E.T. was supported by a terminal-year fellowship from Northwestern University. N.E.T. and J.M.N. acknowledge financial support from the Dow Chemical Company for the synthesis of M-SiO_2 materials. This work was carried out, in part, in the Frederick Seitz Materials Research Laboratory Central Research Facilities at the University of Illinois. This work was supported, in part, by the U.S. Army Research Office under grant number W911NF-16-1-0128 and the National Science Foundation under grant number CBET-1553137.

■ REFERENCES

(1) Guo, Z.; Liu, B.; Zhang, Q.; Deng, W.; Wang, Y.; Yang, Y. Recent advances in heterogeneous selective oxidation catalysis for sustainable chemistry. *Chem. Soc. Rev.* **2014**, *43*, 3480−3524.

(2) Ali, M. E.; Rahman, M. M.; Sarkar, S. M.; Hamid, S. B. A. Heterogeneous Metal Catalysis for Oxidation Reactions. *J. Nanomater.* **2014**, *2014*, 1−23.

(3) Clerici, M. G.; Kholdeeva, O. A. *Liquid Phase Oxidation via Heterogeneous Catalysis: Organic Synthesis and Industrial Applications*; John Wiley & Sons: New York, 2013; Vol. *1*, p 71.

(4) Lehmhus, D.; Busse, M.; Herrmann, A.; Kayvantash, K. *Structural Materials and Processes in Transportation*; Wiley-VCH: Weinheim, Germany, 2013; Vol. *1*, pp 11−17.

(5) Choi, W. J.; Choi, C. Y. Production of Chiral Epoxides: Epoxide Hydrolase-catalyzed Enantioselective Hydrolysis. *Biotechnol. Bioprocess Eng.* **2005**, *10*, 167−179.

(6) Ellis, B. *Chemistry and Technology of Epoxy Resins*; Springer: The Netherlands, 1993; Vol. *1*, p 1.

(7) Thornburg, N. E.; Thompson, A. B.; Notestein, J. M. Perioidic Trends in Highly Dispersed Groups IV and V Supported Metal Oxide Catalysts for Alkene Epoxidation with H_2O_2. *ACS Catal.* **2015**, *5*, 5077−5088.

(8) Thornburg, N. E.; Nauert, S. L.; Thompson, A. B.; Notestein, J. M. Synthesis-Structure-Function Relationships of Silica-Supported Niobium(V) Catalysts for Alkene Epoxidation. *ACS Catal.* **2016**, *6*, 6124−6134.

(9) Bregante, D. T.; Priyadarshini, P.; Flaherty, D. W. Kinetic and spectroscopic evidence for reaction pathways and intermediates for olefin epoxidation on Nb in *BEA. *J. Catal.* **2017**, *348*, 75−89.

(10) Bregante, D. T.; Flaherty, D. W. Periodic Trends in Olefin Epoxidation over Group IV and V Framework-Substituted Zeolite Catalysts: A Kinetic and Spectroscopic Study. *J. Am. Chem. Soc.* **2017**, *139*, 6888−6898.

(11) Wilson, N. M.; Bregante, D. T.; Priyadarshini, P.; Flaherty, D. W. Production and Use of H_2O_2 for Atom-Efficient Functionalization of Hydrocarbons and Small Molecules. *Catalysis* **2017**, *29*, 122−212.

(12) Ethylene Oxide. *Ullman's Encyclopedia of Industrial Chemistry*; Wiley-VCH: Weinheim, Germany, 2012.

(13) Epoxides. *Ullman's Encyclopedia of Industrial Chemistry*; Wiley-VCH: Weinheim, Germany, 2012.

(14) Gleeson, D.; Sankar, G.; Catlow, R. A. C.; Meurig, T. J.; Spanó, G.; Bordiga, S.; Zecchina, A.; Lamberti, C. The architecture of catalytically active centers in titanosilicate (TS-1) and related selective-oxidation catalysts. *Phys. Chem. Chem. Phys.* **2000**, *2*, 4812−4817.

(15) Carati, A.; Flego, C.; Previde Massara, E.; Millini, R.; Carluccio, L.; Parker, W. O.; Bellussi, G. Stability of Ti in MFI and Beta structures: A comparative study. *Microporous Mesoporous Mater.* **1999**, *30*, 137−144.

(16) van Vliet, M. C. A.; Mandelli, D.; Arends, I. W. C. E.; Schuchardt, U.; Sheldon, R. A. Alumina: a cheap, active and selective catalyst for epoxidation with (aqueous) hydrogen peroxide. *Green Chem.* **2001**, *3*, 243−246.

(17) Mandelli, D.; van Vliet, M. C. A.; Sheldon, R. A.; Schuchardt, U. Alumina-catalyzed alkene epoxidation with hydrogen peroxide. *Appl. Catal., A* **2001**, *219*, 209−213.

(18) Wolf, P.; Hammond, C.; Conrad, S.; Hermans, I. Post-synthetic preparation of Sn-, Ti- and Zr-beta: a facile route to water tolerant, highly active Lewis acidic Zeolites. *Dalton Trans.* **2014**, *43*, 4514−4519.

(19) Srinivas, D.; Manikandan, P.; Laha, S. C.; Kumar, R.; Ratnasamy, P. Reactive oxo-titanium species in titanosilicate molecular sieves: EPR investigations and structure-activity correlations. *J. Catal.* **2003**, *217*, 160−171.

(20) Notestein, J. M.; Andrini, L. R.; Kalchenko, V. I.; Requejo, F. G.; Katz, A.; Iglesia, E. Structural Assessment and Catalytic Consequences of the Oxygen Coordination Environment in Grafed Ti-Calixarenes. *J. Am. Chem. Soc.* **2007**, *129*, 1122−1131.

(21) Prasetyoko, D.; Ramli, Z.; Endud, S.; Nur, H. Enhancement of Catalytic Activity of Titanosilicalite-1 − Sulfated Zirconia Combination Towards Epoxidation of 1-Octene with Aqueous Hydrogen Peroxide. *React. Kinet. Catal. Lett.* **2005**, *86*, 83−89.

(22) Ivanchikova, I. D.; Maksimchuk, N. V.; Skobelev, I. Y.; Kaichev, V. V.; Kholdeeva, O. A. Mesoporous niobium-silicates prepared by evaporation-induced self-assembly as catalysts for selective oxidations with aqueous H_2O_2. *J. Catal.* **2015**, *332*, 138−148.

(23) Aronne, A.; Turco, M.; Bagnasco, G.; Ramis, G.; Santacesaria, E.; Di Serio, M.; Marenna, E.; Bevilacqua, M.; Cammarano, C.; Fanelli, E. Gel derived niobium-silicon mixed oxides: Characterization and catalytic activity for cyclooctene epoxidation. *Appl. Catal., A* **2008**, *347*, 179−185.

(24) Ruddy, D. A.; Tilley, T. D. Highly selective olefin epoxidation with aqueous H_2O_2 over surface-modified TaSBA15 prepared *via* the TMP method. *Chem. Commun.* **2007**, 3350−3352.

(25) Ruddy, D. A.; Tilley, T. D. Kinetics and Mechanism of Olefin Epoxidation with Aqueous H_2O_2 and a Highly Selective Surface-Modified TaSBA15 Heterogeneous Catalyst. *J. Am. Chem. Soc.* **2008**, *130*, 11088−11096.

(26) Morlanés, N.; Notestein, J. M. Kinetic study of cyclooctene epoxidation with aqueous hydrogen peroxide over silica-supported calixarene-Ta(V). *Appl. Catal., A* **2010**, *387*, 45−54.

(27) Boronat, M.; Corma, A.; Renz, M.; Viruela, P. M. Predicting the Activity of Single Isolated Lewis Acid Sites in Solid Catalysts. *Chem. - Eur. J.* **2006**, *12*, 7067−7077.

(28) Gallo, A.; Tiozzo, C.; Psaro, R.; Carniato, F.; Guidotti, M. Niobium metallocenes deposited onto mesoporous silica via dry impregnation as catalysts for selective epoxidation of alkenes. *J. Catal.* **2013**, *298*, 77−83.

(29) Tiozzo, C.; Bisio, C.; Carniato, F.; Gallo, A.; Scott, S. L.; Psaro, R.; Guidotti, M. Niobium-silica catalysts for the selective epoxidation of cyclic alkenes: the generation of the active site by grafting niobocene dichloride. *Phys. Chem. Chem. Phys.* **2013**, *15*, 13354−13362.

DOI: 10.1021/acscatal.7b03986
ACS Catal. 2018, 8, 2995−3010

(30) Bérubé, F. O.; Nohair, B.; Kleitz, F.; Kaliaguine, S. Controlled Postgrafting of Titanium Chelates for Improved Synthesis of Ti-SBA-15 Epoxidation Catalysts. *Chem. Mater.* **2010**, *22*, 1988−2000.
(31) Dzwigaj, S.; Millot, Y.; Che, M. Ta(V)-Single Site BEA Zeolite by Two-Step Postsynthesis Method: Preparation and Characterization. *Catal. Lett.* **2010**, *135*, 169−174.
(32) Dzwigaj, S.; Millot, Y.; Méthivier, C.; Che, M. Incorporation of Nb(V) into BEA zeolite investigated by XRD, NMR, IR, DR UV-vis, and XPS. *Microporous Mesoporous Mater.* **2010**, *130*, 162−166.
(33) Tang, B.; Dai, W.; Sun, X.; Guan, N.; Li, L.; Hunger, M. A procedure for the preparation of Ti-Beta zeolites for catalytic epoxidation with hydrogen peroxide. *Green Chem.* **2014**, *16*, 2281−2291.
(34) Giannini, L.; Solari, E.; Zanotti-Gerosa, A.; Floriani, C.; Chiesi-Villa, A.; Rizzoli, C. The Organometallic Chemistry of Zirconium on an Oxo Surface Provided by *p-tert*-Butylcalix[4]arene. *Angew. Chem., Int. Ed. Engl.* **1996**, *35*, 85−87.
(35) Castellano, B.; Solari, E.; Floriani, C.; Re, N.; Chiesi-Villa, A.; Rizzoli, C. Tantalum-Carbon Functionalities Bonded to a Calix[4]-arene-Oxo Matrix: The Chemistry of Mono-, Dialkyl, and Butadiene Derivatives of Tantalum(V). *Chem. - Eur. J.* **1999**, *5*, 722−737.
(36) Caselli, A.; Solari, E.; Scopelliti, S.; Floriani, C.; Re, N.; Rizzoli, C.; Chiesi-Villa, A. Dinitrogen Rearranging over a Metal-Oxo Surface and Cleaving to Nitride: From the End-On to the Side-On Bonding Mode, to the Stepwise Cleavage of the N≡N Bonds Assisted by Nb^{III}-calix[4]arene. *J. Am. Chem. Soc.* **2000**, *122*, 3652−3670.
(37) Zanotti-Gerosa, A.; Solari, E.; Giannini, L.; Floriani, C.; Re, N.; Chiesi-Villa, A.; Rizzoli, C. Titanium-carbon functionalities on an oxo surface defined by a calix[4]arene moiety and its redox chemistry. *Inorg. Chim. Acta* **1998**, *270*, 298−311.
(38) Wang, W.-G.; Zheng, Q.-Y.; Huang, Z.-T. Selective Etherification of Calix[4]arenes. *Synth. Commun.* **1999**, *29*, 3711−3718.
(39) Eaton, T. R.; Boston, A. M.; Thompson, A. B.; Gray, K. A.; Notestein, J. M. Counting Active Sites on Titanium Oxide-Silica Catalysts for Hydrogen Peroxide Activation Through In Situ Poisoning with Phenylphosphonic Acid. *ChemCatChem* **2014**, *6*, 3215−3222.
(40) Wang, J.; Kispersky, V. F.; Delgass, N. W.; Ribeiro, F. H. Determination of the Au active site and surface active species via *operando* transmission FTIR and isotopic transient experiments on 2.3 wt.% Au/TiO_2 for the WGS reaction. *J. Catal.* **2012**, *289*, 171−178.
(41) Barzetti, T.; Selli, E.; Moscotti, D.; Forni, L. Pyridine and ammonia as probes for FTIR analysis of solid acid catalysts. *J. Chem. Soc., Faraday Trans.* **1996**, *92*, 1401−1407.
(42) Kondo, J. N.; Nishitani, R.; Yoda, E.; Yokoi, T.; Tatsumi, T.; Domen, K. A comparative IR characterization of acidic sites on HY zeolite by pyridine and CO probes with silica-alumina and γ-alumina references. *Phys. Chem. Chem. Phys.* **2010**, *12*, 11576−11586.
(43) Müller, P.; Burt, S. P.; Love, A. M.; McDermott, W. P.; Wolf, P.; Hermans, I. Mechanistic Study on the Lewis Acid Catalyzed Synthesis of 1,3-Butadiene over Ta-BEA Using Modulated Operando DRIFTS-MS. *ACS Catal.* **2016**, *6*, 6823−6832.
(44) Madon, R. J.; Boudart, M. Experimental Criterion for the Absence of Artifacts in the Measurement of Rates of Heterogeneous Catalytic Reactions. *Ind. Eng. Chem. Fundam.* **1982**, *21*, 438−447.
(45) Ignacio-de Leon, P. A. A.; Contreras, C. A.; Thornburg, N. E.; Thompson, A. B.; Notestein, J. M. Catalyst structure and substituent effects on epoxidation of styrenics with immobilized Mn(tmtacn) complexes. *Appl. Catal., A* **2016**, *511*, 78−86.
(46) de Boer, J. W.; Browne, W. R.; Harutyunyan, S. R.; Bini, L.; Tiemersma-Wegman, T. D.; Alsters, P. L.; Hage, R.; Feringa, B. L. Manganese catalysed asymmetric *cis*-dihydroxylation with H_2O_2. *Chem. Commun.* **2008**, 3747−3749.
(47) Aimone-Gastin, I.; Cable, S.; Keller, J. M.; Bigard, M. A.; Champigneulle, B.; Gaucher, P.; Gueant, J. L.; Dauça, M. Studies on Peroxisomes of Colonic Mucosa in Crohn's Disease. *Dig. Dis. Sci.* **1994**, *39*, 2177−2185.
(48) Shetti, V. N.; Manikandan, P.; Srinivas, D.; Ratnasamy, P. Reactive oxygen species in epoxidation reactions over titanosilicate molecular sieves. *J. Catal.* **2003**, *216*, 461−467.
(49) Ratnasamy, P.; Srinivas, D.; Knözinger, H. Active Sites and Reactive Intermediates in Titanium Silicate Molecular Sieves. *Adv. Catal.* **2004**, *48*, 1−169.
(50) Ziolek, M.; Sobczak, I.; Decyk, P.; Sobańska, K.; Pietrzyk, P.; Sojka, Z. Search for reactive intermediates in catalytic oxidation reactions with hydrogen peroxide over amorphous niobium(V) and tantalum(V) oxides. *Appl. Catal., B* **2015**, *164*, 288−296.
(51) Bakac, A. *Physical Inorganic Chemistry: Principles, Methods, and Models*; John Wiley & Sons: New York, 2010; Vol. *1*, p 134
(52) Bonino, F.; Damin, A.; Ricchiardi, G.; Ricci, M.; Spanó, G.; D'Aloisio, R.; Zecchina, A.; Lamberti, C.; Prestipino, C.; Bordiga, S. Ti-Peroxo Species in the TS-1/H_2O_2/H_2O System. *J. Phys. Chem. B* **2004**, *108*, 3573−3583.
(53) Bordiga, S.; Damin, A.; Bonino, F.; Ricchiardi, G.; Lamberti, C.; Zecchina, A. The Structure of the Peroxo Species in the TS-1 Catalyst as Investigated by Resonant Raman Spectroscopy. *Angew. Chem., Int. Ed.* **2002**, *41*, 4734−4737.
(54) Bordiga, S.; Groppo, E.; Agostini, G.; van Bokhoven, J. A.; Lamberti, C. Reactivity of Surface Species in Heterogeneous Catalysts Probed by In Situ X-ray Absorption Techniques. *Chem. Rev.* **2013**, *113*, 1736−850.
(55) Yoon, C. W.; Hirsekorn, K. F.; Neidig, M. L.; Yang, X.; Tilley, T. D. Mechanism of the Decomposition of Aqueous Hydrogen Peroxide over Heterogeneous TiSBA15 and TS-1 Selective Oxidation Catalysts: Insights from Spectroscopic and Density Functional Theory Studies. *ACS Catal.* **2011**, *1*, 1665−1678.
(56) Ruddy, D. A.; Brutchey, R. L.; Tilley, T. D. The Influence of Surface Modification on the Epoxidation Selectivity and Mechanism of TiSBA15 and TaSBA15 Catalysts with Aqueous Hydrogen Peroxide. *Top. Catal.* **2008**, *48*, 99−106.
(57) Wang, L.; Xiong, G.; Su, J.; Li, P.; Guo, H. Situ UV Raman Spectroscopic Study on the Reaction Intermediates for Propylene Epoxidation on TS-1. *J. Phys. Chem. C* **2012**, *116*, 9122−9131.
(58) Oyama, S. T. In *Mechanisms in Homogeneous and Heterogeneous Epoxidation Catalysis*; Elsevier: Amsterdam, 2008; Vol *1*, pp 3−99.
(59) Bayot, D.; Devillers, M. Peroxo complexes of niobium(V) and tantalum(V). *Coord. Chem. Rev.* **2006**, *250*, 2610−2626.
(60) Bayot, D.; Tinant, B.; Devillers, M. Water-soluble niobium peroxo complexes as precursors for the preparation of Nb-based oxide catalysts. *Catal. Today* **2003**, *78*, 439−447.
(61) Sergienko, V. S. Structural Characteristics of Peroxo Complexes of Group IV and V Transition Metals. Review. *Crystallogr. Rep.* **2004**, *49*, 907−929.
(62) Knops-Gerrits, P.; De Vos, D.; Feijen, E. J. P.; Jacobs, P. A. Raman spectroscopy on zeolites. *Microporous Mater.* **1997**, *8*, 3−17.
(63) Ivanchikova, I. D.; Skobelev, I. Y.; Maksimchuk, N. V.; Paukshtis, E. A.; Shashkov, M. V.; Kholdeeva, O. A. Toward understanding the unusual reactivity of mesoporous niobium silicates in epoxidation of C = C bonds with hydrogen peroxide. *J. Catal.* **2017**, *356*, 85−99.
(64) Khouw, C. B.; Dartt, C. B.; Labinger, J. A.; Davis, M. E. Studies on the Catalytic Oxidation of Alkanes and Alkenes by Titanium Silicates. *J. Catal.* **1994**, *149*, 195−205.
(65) Stare, J.; Henson, N. J.; Eckert, J. Mechanistic Aspects of Propene Epoxidation by Hydrogen Peroxide. Catalytic Role of Water Molecules, External Electric Field, and Zeolite Framework of TS-1. *J. Chem. Inf. Model.* **2009**, *49*, 833−846.
(66) Clerici, M. G.; Ingallina, P. Epoxidation of Lower Olefins with Hydrogen Peroxide and Titanium Silicalite. *J. Catal.* **1993**, *140*, 71−83.
(67) Kurti, L.; Czako, B. *Strategic Applications of Named Reactions in Organic Synthesis*; Academic Press: San Diego, CA, 2005; Vol. *1*, p 362.
(68) Deubel, D. V.; Sundermeyer, J.; Frenking, G. Mechanism of the Olefin Epoxidation Catalyzed by Molybdenum Diperoxo Complexes: Quantum-Chemical Calculations Give an Answer to a Long-Standing Question. *J. Am. Chem. Soc.* **2000**, *122*, 10101−10108.

DOI: 10.1021/acscatal.7b03986
ACS Catal. 2018, 8, 2995−3010

(69) Raj, N. K. K.; Ramaswamy, A. V.; Manikandan, P. Oxidation of norbornene over vanadium-substituted phosphomolybdic acid catalysts and spectroscopic investigations. *J. Mol. Catal. A: Chem.* **2005**, *227*, 37−45.
(70) Kuznetsov, M. L.; Pessoa, J. C. Epoxidation of olefins catalysed by vanadium-salan complexes: a theoretical mechanistic study. *Dalton Trans.* **2009**, 5460−5468.
(71) Flaherty, D. W.; Iglesia, E. Transition-State Enthalpy and Entropy Effects on Reactivity and Selectivity in Hydrogenolysis of *n*-Alkanes. *J. Am. Chem. Soc.* **2013**, *135*, 18586−99.
(72) Anslyn, E. V.; Dougherty, D. A. *Modern Physical Organic Chemistry*; University Science Books: Mill Valley, CA, 2005; Vol. *1*, p 445.
(73) Gounder, R.; Iglesia, E. The catalytic diversity of zeolites: confinement and solvation effects within voids of molecular dimensions. *Chem. Commun.* **2013**, *49*, 3491−509.
(74) First, E. L.; Gounaris, C. E.; Wei, J.; Floudas, C. A. Computational characterization of zeolite porous networks: an automated approach. *Phys. Chem. Chem. Phys.* **2011**, *13*, 17339−17358.
(75) Bienert, G. P.; Schjoerring, J. K.; Jahn, T. P. Membrane transport of hydrogen peroxide. *Biochim. Biophys. Acta, Biomembr.* **2006**, *1758*, 994−1003.
(76) Corma, A.; Garcia, H. Lewis Acids as Catalysts in Oxidation Reactions: From Homogeneous to Heterogeneous Systems. *Chem. Rev.* **2002**, *102*, 3837−3892.
(77) Notari, B. Microporous Crystalline Titanium Silicates. *Adv. Catal.* **1996**, *41*, 253−334.
(78) Gounder, R.; Davis, M. E. Monosaccharide and disaccharide isomerization over Lewis acid sites in hydrophobic and hydrophilic molecular sieves. *J. Catal.* **2013**, *308*, 176−188.
(79) Gounder, R. Hydrophobic microporous and mesoporous oxides as Brønsted and Lewis acid catalysts for biomass conversion in liquid water. *Catal. Sci. Technol.* **2014**, *4*, 2877−2886.
(80) Guidotti, M.; Batonneau-Gener, I.; Gianotti, E.; Marchese, L.; Mignard, S.; Psaro, R.; Sgobba, M.; Ravasio, N. The effect of silylation on titanium-containing silicate catalysts for the epoxidation of functionalised molecules. *Microporous Mesoporous Mater.* **2008**, *111*, 39−47.
(81) Lin, K.; Pescarmona, P. P.; Houthoofd, K.; Liang, D.; Van Tendeloo, G.; Jacobs, P. A. Direct room-temperature synthesis of methyl-functionalized Ti-MCM-41 nanoparticles and their catalytic performance in epoxidation. *J. Catal.* **2009**, *263*, 75−82.

DOI: 10.1021/acscatal.7b03986
ACS Catal. 2018, 8, 2995−3010